applied sciences

MDPI

Article

Pit Limit Optimization for Open-Pit Coal Mines in Fire-Affected Zones: A Case Study of the First Mining Area in Dananhu No. 2 Coal Mine, Xinjiang

Yifang Long [1], Ziling Song [1,2,*], Yu Wen [1] and Kun Zhang [3]

[1] College of Mining, Liaoning Technical University, Fuxin 123000, China; 13579923611@163.com (Y.L.); wyddd324@gmail.com (Y.W.)
[2] College of Environmental Science and Engineering, Liaoning Technical University, Fuxin 123000, China
[3] China Coal Pingshuo Group Co., Ltd., Shuozhou 036000, China; z17856000842@163.com
* Correspondence: songziling-163@163.com

Abstract

Spontaneous combustion in fire-affected coal seams can degrade coal quality, alter rock mechanical parameters and reduce mining profitability. Traditional pit limit optimization methods ignore coal fire-induced quality degradation, ignore the coupling effect of economic fluctuation and slope stability, and lack quantitative optimization for fire-affected open-pit mines. Here, we optimize loss-reducing mining boundaries for the southern fire-affected highwall in the first mining district of the Dananhu No. 2 Mine, Hami, Xinjiang. The aim is to move beyond binary decisions that either sterilize or fully extract fire-affected reserves. We instead integrate economic return, slope stability and coal-price uncertainty into a single boundary-optimization framework. First, we established a three-dimensional Cartesian coordinate system for the study area. We then modeled and fitted the coal-seam roof and floor using MATLAB-based multiple integration, reducing edge errors in solid surfaces. Laboratory analyses of borehole coal samples defined how calorific value varied with advance distance. These data were used to derive the coal-quality curve. Net mining profit was then formulated as the objective function, replacing the conventional stripping-ratio criterion. Profit was calculated across advance distances to identify the economically optimal boundary. Mechanical parameters of thermally altered rocks were obtained from laboratory deformation tests. Rhino and FLAC3D 6.0 were then used to evaluate three-dimensional slope stability at critical locations. Coal-price perturbation scenarios were finally introduced to test the sensitivity of net profit and optimal advance distance. Under the baseline coal price, the slope remained stable at an advance distance of 193 m. At this boundary, net profit reached a maximum of RMB 676.608 million. The southern surface boundary contracted by 47 m relative to the initial boundary, reducing unnecessary land disturbance. Sensitivity analysis showed that lower coal prices sharply reduced both the optimal advance distance and maximum net profit. When coal price decreased by 30%, the optimal advance distance contracted to approximately 116.9 m. Maximum net profit fell to approximately RMB 248.239 million. Higher coal prices expanded the optimal boundary outward. Once coal price reached approximately 128.7 yuan/t, or 18.5% above baseline, the optimum reached the upper constraint of 240 m. Net profit then increased substantially with further price growth. These results provide a quantitative basis for dynamic boundary optimization and disturbance-reducing extraction in fire-affected open-pit coal mines.

Check for updates

Academic Editor: Antonio Bernardo Sánchez

Received: 4 June 2026
Revised: 12 July 2026
Accepted: 5 August 2026
Published: 25 August 2026

Copyright: © 2026 by the authors. Licensee MDPI, Basel, Switzerland. This article is an open access article distributed under the terms and conditions of the Creative Commons Attribution (CC BY) license.

Keywords: open-pit coal mine; fire-affected zone; boundary optimization; loss-mitigation mining; slope stability; net profit

1. Introduction

Open-pit mining areas in Northwest China are widely affected by coal fire zones, particularly in the coal-rich Xinjiang region. The arid climatic conditions and shallow burial of coal seams in this area significantly increase the susceptibility of coal spontaneous combustion, resulting in the formation of large-scale coal fire areas [1]. Coal spontaneous combustion not only severely degrades the calorific value of coal resources but also induces prominent variations in the physical and mechanical properties of overlying and surrounding rock masses under long-term high-temperature thermal action. This process forms thermally altered burnt rock with substantially reduced shear strength and poor structural integrity [2]. In practical open-pit coal mining engineering, conventional treatment strategies for coal-fire-overlying areas generally fall into two extreme categories. To guarantee slope stability and control the economic stripping ratio, abandoned mining of coal resources in fire-affected zones is commonly adopted, which leads to enormous waste of valuable coal resources. In contrast, full boundary mining implemented strictly in accordance with the original design not only causes economic losses due to the poor quality of spontaneous combustion coal and consequent cost inversion but also greatly increases the risk of end-slope landslides. Such geological hazards are primarily triggered by the large-area exposure and disturbance of fractured burnt rock masses. Accordingly, the scientific determination of reasonable mining boundaries for coal fire zones is a critical and urgent engineering problem to be solved for the safe, efficient, and sustainable exploitation of open-pit coal resources [3].

Open-pit boundary optimization constitutes the core fundamental research of open-pit mining engineering. In recent years, the relevant optimization theories and techniques have evolved from the initial static geometric optimization into a sophisticated dynamic optimization framework with multi-factor constraints and multi-objective coordination. Conventional open-pit limit optimization methods generally assume uniform coal quality and intact rock mechanical parameters unaffected by thermal damage. However, coal spontaneous combustion zones feature spatially gradual attenuation of coal calorific value and severe degradation of rock strength. Lacking a quantitative module to characterize coal quality deterioration, traditional models fail to simultaneously account for thermally altered rock parameters and fluctuating coal prices, making them unsuitable for mines with coal fire hazards Xu et al. [4] established a multi-objective optimization model for open-pit mining boundaries that integrates economic benefits, ecological costs and social performance. Considering dynamic market constraints, Wang et al. [5] proposed a medium- and long-term dynamic optimization approach accounting for coal price fluctuations, which effectively enhances the operational risk resistance of open-pit mines under volatile market environments. Aiming at complex geological conditions and variable seam occurrence characteristics, Zhang et al. [6] investigated the collaborative mining technology and boundary optimization strategy for marginal and stagnant coal resources in open-pit coal mines. Meanwhile, Lv et al. [7] developed a dynamic collaborative optimization and decision-making method for pit-bottom boundaries of open-pit mines with multi-seam composite structures. The above studies have significantly improved and enriched the theoretical system of open-pit boundary optimization under complex engineering constraints.

Nevertheless, for the special engineering geological scenario of coal fire zones, existing studies predominantly focus on early disaster detection and late-stage governance measures.

Li et al. [8] proposed a high-precision identification method for the spatial boundary of coal fire zones based on deep learning. Song et al. [9] revealed the physical and mechanical characteristics of burnt rock masses and optimized the corresponding blasting parameters. In terms of mining boundary decision making, Cao et al. [10] explored a zonal boundary optimization method for inclined-seam open-pit coal mines under burnt rock erosion conditions, providing a novel perspective for boundary determination of coal fire areas. However, systematic quantitative optimization and decision-making theories targeting coal fire zones remain insufficiently established. Traditional boundary optimization models generally assume uniform spatial distribution of coal calorific value and stable mechanical parameters of rock masses, which cannot be directly applied to the complex coupled scenarios in fire-affected areas characterized by sharp nonlinear degradation of coal calorific value and significant weakening of rock mass strength.

Against this background, this study addresses the core scientific problem of constructing a quantitative coupling mechanism among the spatial degradation law of coal calorific value, the weakening characteristics of slope rock mass mechanical parameters, and mining net profit in coal fire zones. On this basis, the optimal three-dimensional dynamic mining boundary is determined under the dual constraints of economic benefit and slope stability. Taking the southern slope coal fire zone in the first mining area of the Dananhu No. 2 Open-Pit Coal Mine in Xinjiang as the engineering background, this study establishes a spatial function of coal quality degradation and a net-profit objective model to propose a solution framework for the economically optimal mining advance rate. Furthermore, a three-dimensional numerical simulation is adopted to verify slope stability, forming a two-layer mining decision framework of economic optimization and safety verification. Finally, a sensitivity analysis under fluctuating coal price scenarios is conducted. This study aims to break through the traditional extreme mining strategies of full abandonment or complete exploitation and realize the coordinated optimization of economic benefits and slope stability for open-pit mining in coal fire zones.

2. Materials and Methods

2.1. Modeling Assumptions

Coal seam spatial morphology is expressed by continuous quadratic fitting surfaces fitted via MATLAB (R2023b; MathWorks, Natick, MA, USA) multiple integration; edge errors of solid models are controlled, and stratigraphic layers are regarded as horizontally stable without local abrupt tectonic mutation within the research range.

2.2. Overview of the Study Area

The Dananhu No. 2 Open-Pit Coal Mine (hereinafter referred to as Dananhu No. 2 Mine), located in the western block of the Dananhu mining area, under the jurisdiction of Guoshen Hami Coal Power Company of the China Energy Investment Corporation, is administratively affiliated with Nanhu Township, Hami city, Xinjiang Uygur Autonomous Region. The mine is approximately 84 km away from the urban area of Hami city and 45 km from Nanhu Township. According to the production capacity of mining equipment and the designed annual output, the mining area is divided into four independent mining panels. The first mining panel is situated in the central part of the mining area, with its southern slope adjacent to the No. III coal fire zone, and the designed service life of the mine is 44 years. The southern slope is categorized as a subhorizontal layered slope. Coal seams are buried at depths ranging from 10 to 20 m with a dip angle of approximately 5°, dipping southward to northward. The stratigraphic sequence primarily comprises Quaternary and Jurassic strata. The Quaternary succession consists of loess, sub-sandy soil, and fine silty sand and gravel, whereas the Jurassic strata are dominated by sandy

mudstone, mudstone, coal seams, siltstone, coarse sandstone and medium–fine sandstone. The Quaternary unconsolidated deposits distributed on the southern slope of the initial mining panel are permeable aquitards with no stable water storage capacity. Jurassic strata feature weak water yield properties. Fracture water hosted within these strata is predominantly recharged by atmospheric precipitation and ephemeral surface runoff converged from surrounding terrain. Such groundwater migrates toward the open-pit bottom and discharges onto the pit floor through dispersed fracture seepage, accompanied by weak artesian pressure characteristics. The No. III burnt rock zone is mainly governed by the Nanhu anticline, as well as land surface geomorphology shaped by erosion prior to and after coal spontaneous combustion. This burnt zone wedges into the coal-bearing strata, and the boundaries of the thermally altered rock mass exhibit highly irregular configurations. The geographical location of the Dananhu No. 2 Open-Pit Coal Mine is illustrated in Figure 1 [11].

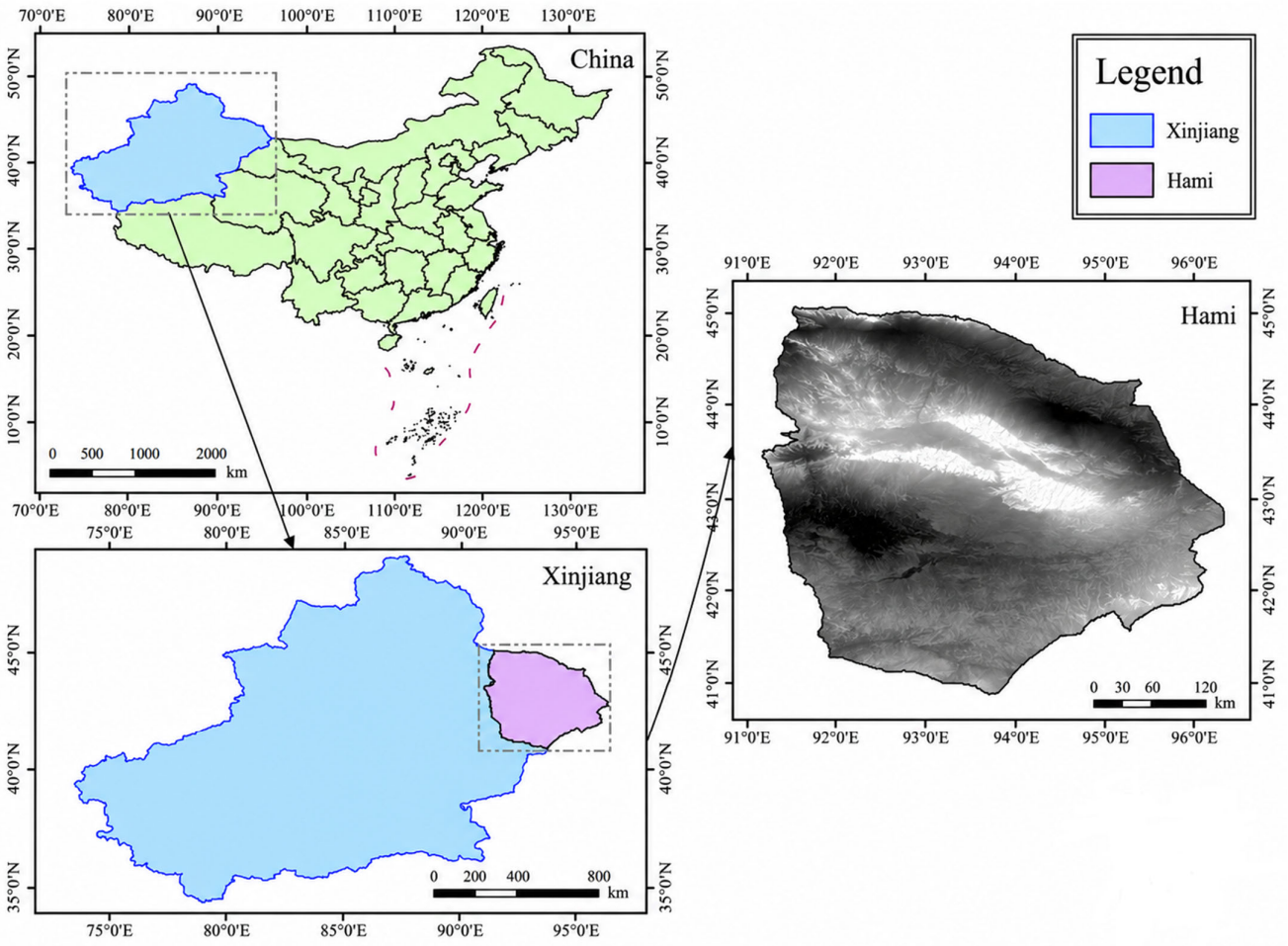


Figure 1. Geographical location map of the Dananhu No. 2 coal mine.

At present, the first mining panel has officially entered the internal dumping stage. The main minable coal seams in this area include the well-developed No. 16, No. 18, No. 21, No. 25 and No. 29 coal seams [12]. Among them, the No. 16 and No. 18 coal seams outcrop on the southern slope, resulting in localized coal spontaneous combustion zones, which further cause severe coal quality deterioration in the deep coal seams. Abandoning the extraction of the No. 16 and No. 18 coal seams will inevitably lead to the loss and waste of the underlying No. 21, No. 25 and No. 29 coal resources on the southern slope. Conversely, mining these two burnt coal seams cannot guarantee positive economic benefits due to coal quality degradation. In addition, affected by the irregular terrain and unstable

slope conditions of the fire zone, the internal dump cannot closely follow and coordinate with stope advancement, which seriously restricts normal mining operations and on-site production efficiency [13,14]. Therefore, it is urgent to carry out targeted research on the mining optimization of end-slope coal fire zones in the first mining panel of the Dananhu No. 2 Open-Pit Coal Mine. The relative positional relationship between the current mining status of the first mining panel and the No. III coal fire zone is shown in Figure 2.

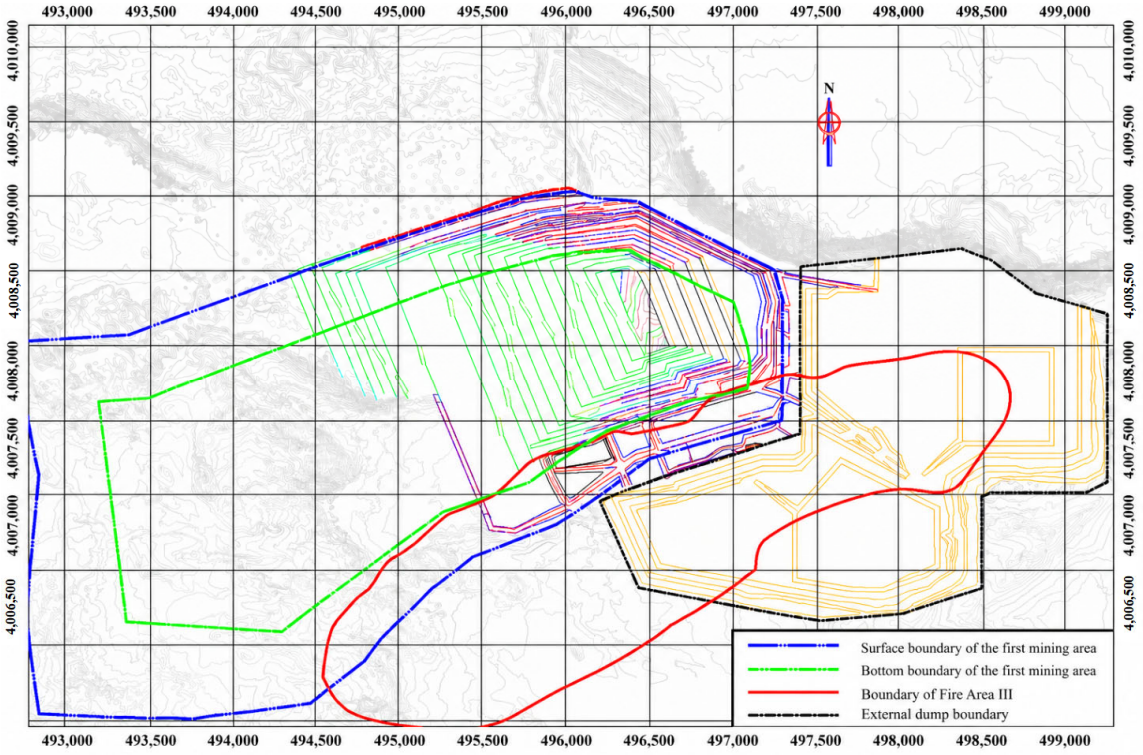


Figure 2. Mining status of the first mining area in 2024 and the No. III burned area.

2.3. Optimization Mining Model for Coal Fire Zones

The stripping operation in the first mining panel of the Dananhu No. 2 Open-Pit Coal Mine has extended into the No. III coal fire zone, which severely restricts regular mining activities and reduces economic benefits. To formulate a reasonable mining optimization scheme for fire-affected areas, it is essential to determine the feasible mining boundary of the coal fire zone. Two extreme mining scenarios are established to simulate and compare the variations in the deep mining boundary of the first mining panel. In the first scenario, considering the degraded coal quality of the spontaneous combusted No. 16 and No. 18 coal seams and the reduced slope stability caused by the deterioration of the rock mechanical parameters, the coal resources overlaid by the No. III coal fire zone on the southern end slope are completely abandoned. In the second scenario, full boundary mining of the No. 16 and No. 18 coal seams on the end slope is implemented in accordance with the original preliminary design. For both scenarios, the end-slope angle is maintained at the designed value of 25° [15]. A comparison of the deep mining boundaries under the two mining modes is presented in Figure 3.

Based on the aforementioned two mining schemes, the professional mine engineering software 3Dmine (Version 2021; Dmine Software, Wuhan, China) was adopted to estimate the resource reserves of the main coal seams affected by the overburden of the No. III coal fire zone. The detailed coal quantity statistics are listed in the following Table 1.

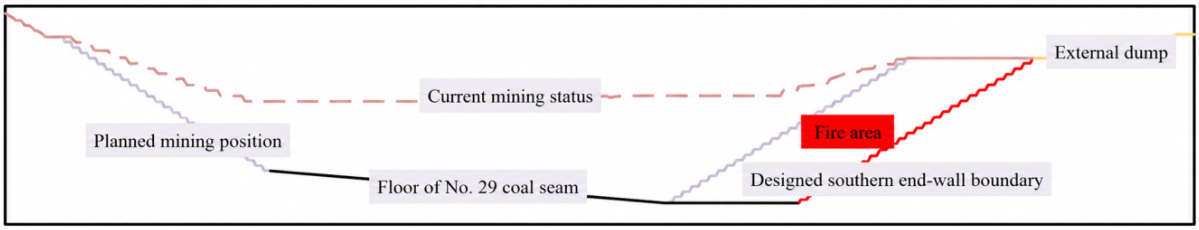


Figure 3. Comparison of the boundaries of different mining modes.

Table 1. Ore and rock mass scale in the study area.

Ore and Rock Type	Volume/m^3	Mass/t	Average Stripping Ratio/$m^3 \cdot t^{-1}$
Rock	128,500,050	282,700,116.1	2.13
No. 16 coal	4,659,275	6,243,428.66	
No. 18 coal	2,234,225	2,993,861.57	
No. 21 coal	4,113,950	5,512,693.14	
No. 25 coal	18,983,400	25,437,756.63	
No. 29 coal	15,075,100	20,200,634.5	
Spontaneous combustion coal	6,893,500	9,237,290.23	
Normal coal	38,172,450	51,151,084.27	

As indicated by the statistical results, the southern end slope of the first mining panel covers over 50.00 Mt of conventional minable coal resources and nearly 10.00 Mt of coal resources with varying spontaneous combustion degrees.

3. Results and Analysis

3.1. Multivariate Function Fitting of Coal Seam Roof and Floor

The above analysis demonstrates that a large amount of coal resources are overlaid in the southern end slope of the first mining panel of the Dananhu No. 2 Open-Pit Coal Mine. Affected by spontaneous combustion at the outcrops of the uppermost No. 16 and No. 18 coal seams, the coal quality of these two seams deteriorates to varying degrees, and the mechanical properties of the surrounding rock masses are significantly degraded due to long-term high-temperature thermal damage. The extraction of the underlying main coal seams (No. 21, No. 25, and No. 29) is also severely restricted by thermally altered burnt rock masses. If mining is strictly implemented in accordance with the original designed slope parameters, two potential risks will occur. Full boundary mining of the No. 16 and No. 18 coal seams will increase production costs due to continuous coal quality degradation, which fails to achieve optimal economic benefits. Excessive mining will expand the exposure area of fractured burnt rock masses, inducing slope instability of the southern end slope and causing extensive land disturbance [16,17]. In accordance with the green and low-loss mining principle for open-pit mines, the rational exploitation of fire-affected coal seams and the efficient recovery of underlying main coal resources have become urgent technical problems to be solved.

Due to coal quality degradation caused by spontaneous combustion at the outcrops of the No. 16 and No. 18 coal seams, the market price of mined coal in this zone is lower than that of normal coal resources. In contrast, the underlying No. 21 coal seam retains favorable coal quality. Therefore, simply adopting the stripping-to-ore ratio to evaluate mining economic efficiency is one-sided and inaccurate. This study incorporates the quality degradation characteristics of spontaneous combusted No. 16 and No. 18 coal seams and the high-quality characteristics of the underlying No. 21, No. 25, and No. 29 coal seams, ensuring that the total economic benefits generated by mined coal resources can cover

the overall stripping and transportation costs. For slope stability control, the significant mechanical deterioration of burnt rock masses easily induces slope failure. Accordingly, slope stability is regarded as the primary constraint, while economic benefit is taken as the secondary optimization objective, to comprehensively clarify the coupling relationship between boundary mining position, slope stability and economic performance [18,19].

In this study, a net profit function is established for the main coal seams including No. 16, No. 18, No. 21, No. 25, and No. 29. The optimal mining advance rate is determined by calculating the net profit corresponding to each mining position. Combined with the slope stability constraint, the optimal mining boundary of the southern end slope is comprehensively optimized to maximize economic benefits and determine the optimal deep mining limit. Net profit is selected as the main economic indicator, and it is briefly compared with other common economic evaluation indicators such as static profit.

In block modeling, a smaller block size contributes to higher modeling accuracy but requires larger data storage capacity and reduces computational efficiency. In general, the block dimension is determined by orebody scale, geological characteristics and mining methods. A complete block model is composed of numerous stacked rectangular blocks, and sub-block division is usually adopted at the mine field boundary to fit the actual morphological characteristics of coal seams. Nevertheless, inevitable errors still exist in boundary constraint processing, especially for coal seams with complex occurrence conditions [20].

Given the stable occurrence conditions of main coal seams in the southern end slope of the Dananhu No. 2 Open-Pit Coal Mine, multiple integral calculations are conducted in this study to estimate coal reserves within the mining boundary before and after optimization. To achieve an accurate reserve calculation for each mining stage, multivariate function fitting is performed for the ground surface and coal seam roof and floor. A three-dimensional rectangular coordinate system is established in the first octant based on the constructed roof and floor surface models of the main coal seams. A total of 80 sets of three-dimensional coordinate points are extracted for both the roof and floor layers. Considering the partial stripping of the original ground surface in the study area, 144 sets of three-dimensional coordinate points are collected to optimize the surface model accuracy. The elevation model of the coal seam roof and floor is shown in Figure 4.

The acquired three-dimensional coordinate data were imported into MATLAB for polynomial fitting of the coal seam roof and floor surfaces. To ensure that the fitting results can accurately reflect the actual occurrence characteristics of the coal seams while effectively avoiding overfitting problems, the quadratic polynomial was selected as the highest fitting order for all surface models. The fitting results of the roof and floor for each main coal seam are illustrated in the corresponding figures. Taking the roof of the No. 18 coal seam as a typical example, the fitting effect is presented in Figure 5.

Accordingly, the dependence of the established response functions of the No. 18 coal seam roof and floor on the two prediction factors can be quantitatively described by the following equations:

$$Z = 384.7966 + 0.0446x - 0.0099y - 0.0001x^2 + 6.4436e^{-6}y^2 \quad (1)$$

$$Z = 382.9210 + 0.0432x - 0.0113y - 0.0001x^2 + 5.7124e^{-6}y^2 \quad (2)$$

$$Z = 409.7966 + 0.04446x - 0.0099y - 0.0001x^2 + 6.44436 \times 10^{-6}y^2 \quad (3)$$

$$Z = 407.9210 + 0.04332x - 0.01113y - 0.0001x^2 + 5.7124 \times 10^{-6}y^2 \quad (4)$$

Among them, Equation (1) represents the variation law of the response function for the No. 18 coal seam roof, and Equation (2) corresponds to the response function of the No.

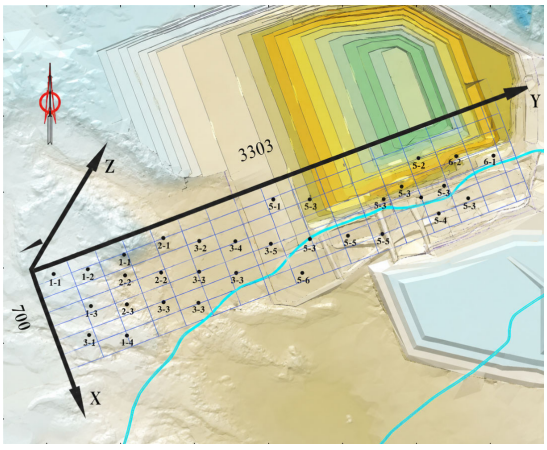
18 coal seam floor. Equation (3) describes the variation characteristics of the fitting response function of the roof of Seam 16, while Equation (4) corresponds to the floor of Seam 16. The fitted surface function of the end-slope boundary under the original preliminary design is expressed as follows:

$$Z = 93.5846 + 0.4663x \quad (5)$$

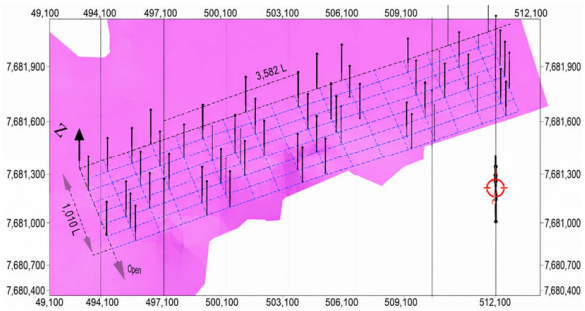
The fitted surface function of the current in situ stope end-slope boundary is defined as follows:

$$Z = 205.4966 + 0.4663x \quad (6)$$

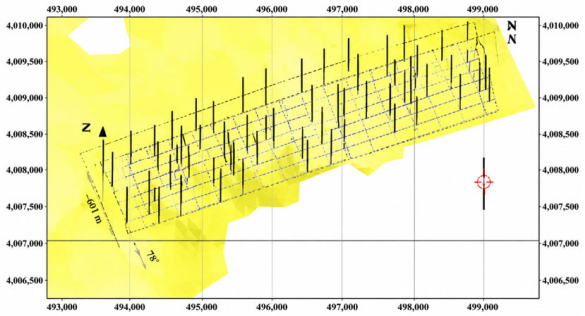
The roof and floor fitting functions of other coal seams are derived in the same manner and are not elaborated herein.



(**a**) 3D coordinate construction of the study area

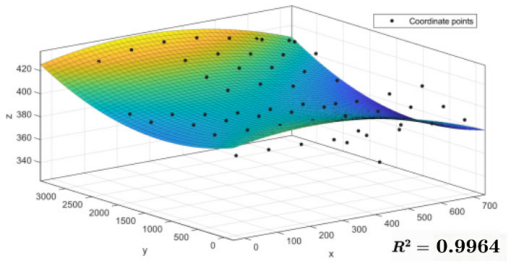


(**b**) Extraction of the roof elevation points

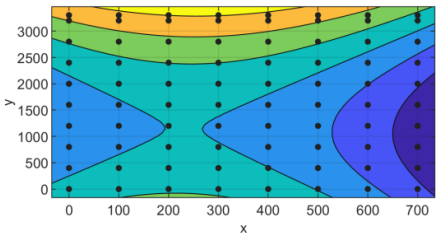


(**c**) Extraction of the floor elevation points

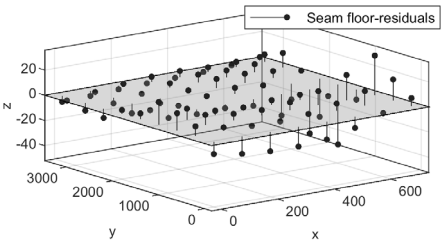
Figure 4. Construction of the three-dimensional coordinate system and extraction of the elevation points of the coal seam roof and floor.



(**a**) No. 18 coal seam roof surface



(**b**) Contour map



(**c**) Residual plot

Figure 5. Fitting surface of the No. 18 coal seam roof.

3.2. Coal Quality Model

To maximize the economic benefits of southern end-slope mining, this study introduces the coal quality variation characteristics of spontaneous combusted No. 16 and No. 18 coal seams. Different from the conventional evaluation method that solely relies on the economic reasonable stripping ratio, this model takes the quality of intact coal as the reference standard. By quantifying the variation in calorific value caused by coal spontaneous combustion in the No. 16 and No. 18 coal seams within the study area, the actual coal quality distribution of the fire-affected zone is determined. Correspondingly, the dynamic coal price corresponding to variable coal quality is calibrated, and the economic benefit variation curve for mining the fire-affected area is further established [21].

The distribution of boreholes adopted for geological exploration and supplementary exploration in the study area is illustrated in Figure 6.

Coal sampling and quality testing were carried out in the shallow outcrop area of the southern end slope for different zones of the No. 16 and No. 18 coal seams to obtain accurate coal quality indicators of fire-affected coal seams.

First, fresh coal samples were collected from newly exposed coal walls in non-combusted and non-weathered working slopes following the national standard GB/T 482-2008 Method for Coal Sampling [22], which were taken as standard reference samples. All field samples were strictly sealed on-site and transported to the laboratory for subsequent testing. After delivery, the coal samples were crushed, sieved, and sealed in self-sealing bags with different particle sizes according to the requirements of various experimental tests for standby application.

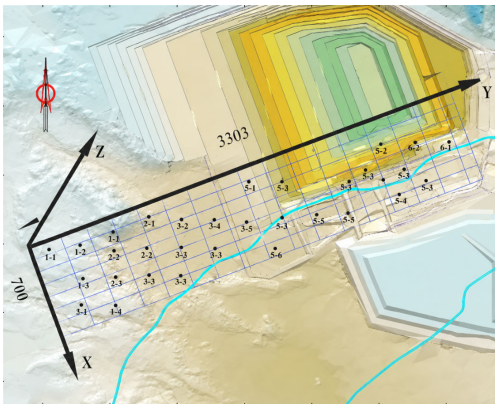


Figure 6. Drilling location.

In accordance with Determination of Calorific Value of Coal, the standard gross calorific values on an air-dried basis (Qgr,ad) of the intact No. 16 and No. 18 coal seams in the working slope were determined to be 23.36 MJ/kg and 24.07 MJ/kg, respectively. Based on the field borehole data of the southern end slope, coal quality samples of the fire-affected No. 16 and No. 18 coal seams were extracted for five-component industrial analysis of the coal. For each borehole position, the average value of three parallel sample tests was adopted as the representative gross calorific value to characterize the spatial variation in the coal calorific value in the fire-affected zone [23]. The calorific value distribution of borehole sampling points is shown in Figure 7.

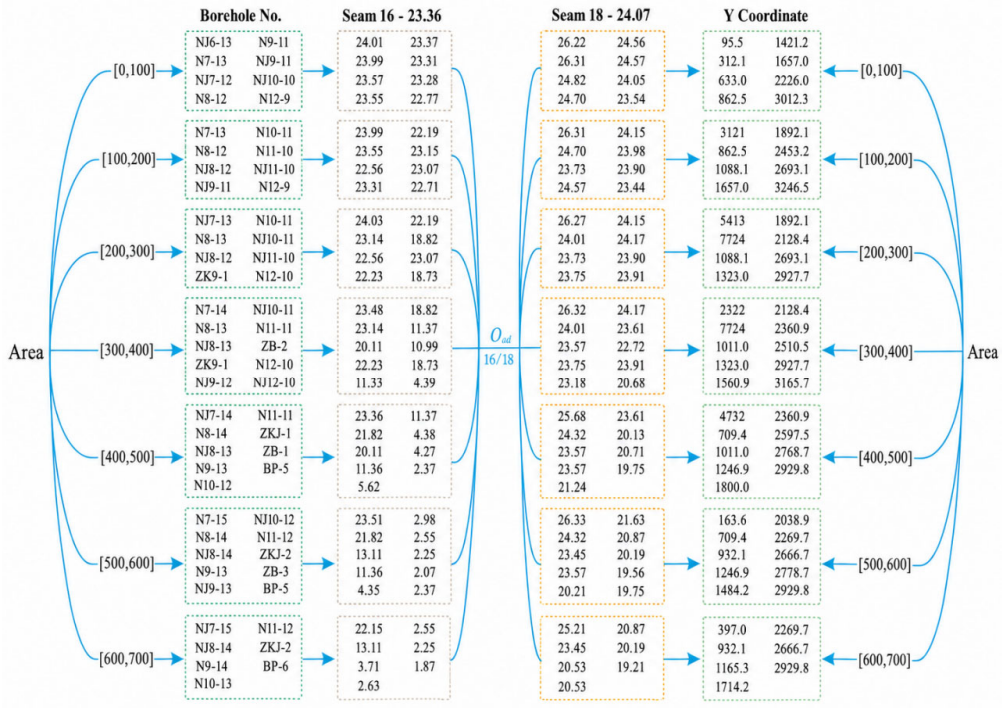


Figure 7. Regional borehole heat generation.

The calorific value data of each borehole were converted and corrected based on the measured coal quality parameters of fresh working slope coal samples to establish the spatial variation curves of the coal quality for the No. 16 and No. 18 coal seams in the study area. In the data conversion process, sampling points with calorific values up to the standard of the intact coal were assigned a correction coefficient of one, while points with degraded calorific values were converted proportionally according to the measured standard calorific value. The corrected calorific value was adopted to quantitatively char-

acterize the actual heat generation capacity of coal seams in fire-affected zones [24]. The spatial variation characteristics of the coal quality in different regions are presented in Figure 8.

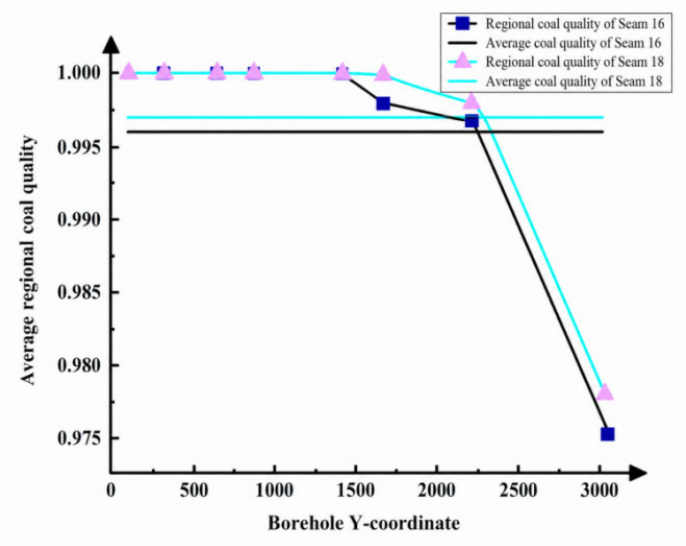
The air-dried basis calorific value (Qad) data obtained from borehole tests in the study area were fitted into a three-dimensional polynomial function to simulate the spatial variation in coal quality along the *X*-axis direction within the research zone. The fitted function curve is displayed in Figure 9.

It can be observed from the above figure that both the No. 16 and No. 18 coal seams suffer from spontaneous combustion to varying degrees. Affected by its elevation distribution characteristics, the No. 16 coal seam exhibits dramatic coal quality fluctuations along the mining direction, with the coal quality correction coefficient ranging from 0.25 to 1. As the underlying coal seam of the No. 16 coal seam, the No. 18 coal seam is also partially affected by spontaneous combustion, whereas its overall coal quality fluctuation is relatively slight, with the correction coefficient stably varying between 0.9 and 1. Taking the No. 16 and No. 18 coal seams with the most severe spontaneous combustion as the research objects, the fitted roof and floor surfaces and corresponding coal quality variation curves of the two coal seams are presented in Figure 10.

Based on the fitted surface functions of coal seam roofs and floors, the multiple integral method is adopted to calculate the stripped rock volume and total coal resource tonnage within the study area. Prior to the volume integration calculation, the *X*-axis coordinates of the intersection lines between each fitted surface and the designed final slope boundary are determined, and the corresponding results are illustrated in Figure 11.

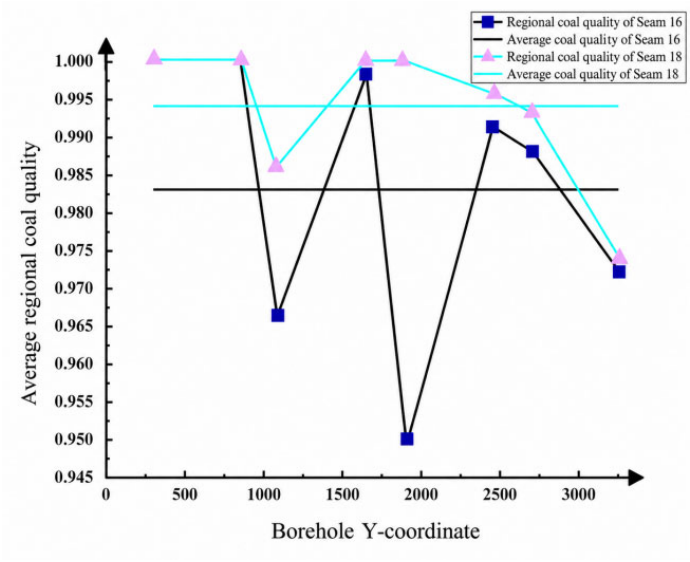
Taking the overburden stripping above the No. 16 coal seam and the mining of the No. 16 coal seam as a typical calculation example, the overburden stripping volume above the No. 16 coal seam is calculated as follows:

$$V_{bt} = \int_{0}^{3303} \int_{x_1}^{x_1'} (68.3867 - 0.1057x - 3.17e^{-2}y + e^{-4}x^2 + 6.225e^{-6}y^2)\,dx\,dy$$
$$x_1' = x_1 + \Delta x; \quad (7)$$
$$x_1 = \frac{\sqrt{5111y^2 - 9.3e^6y + 6.299184e^{11}}}{100\sqrt{10}} - 2067;$$

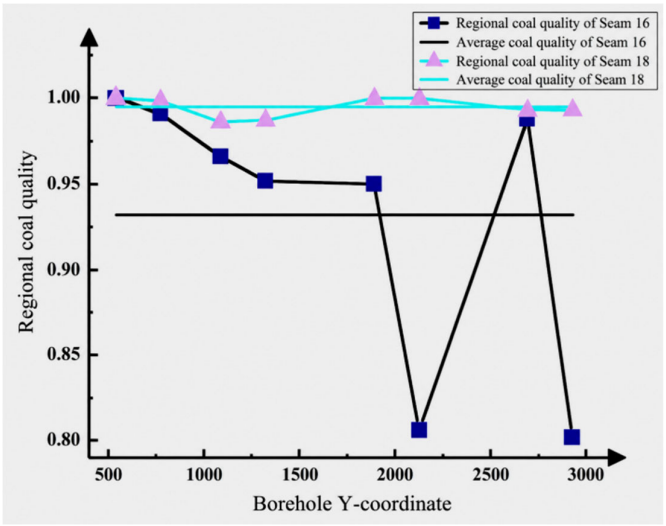


(**a**) Region [0, 100]

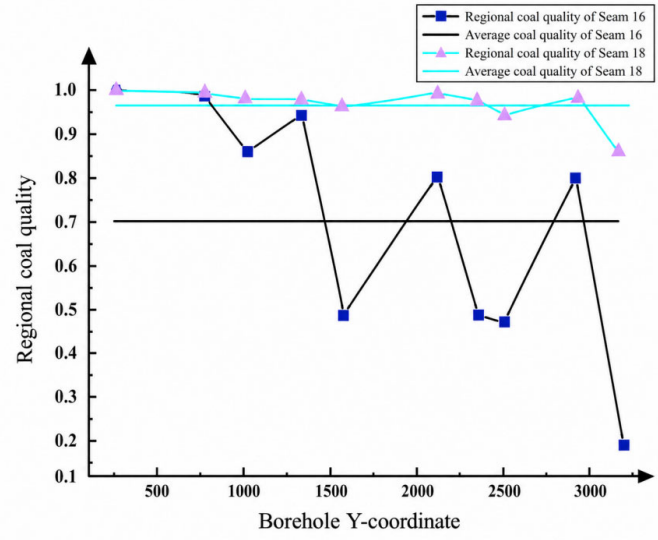
Figure 8. *Cont.*



(**b**) Region [100, 200]

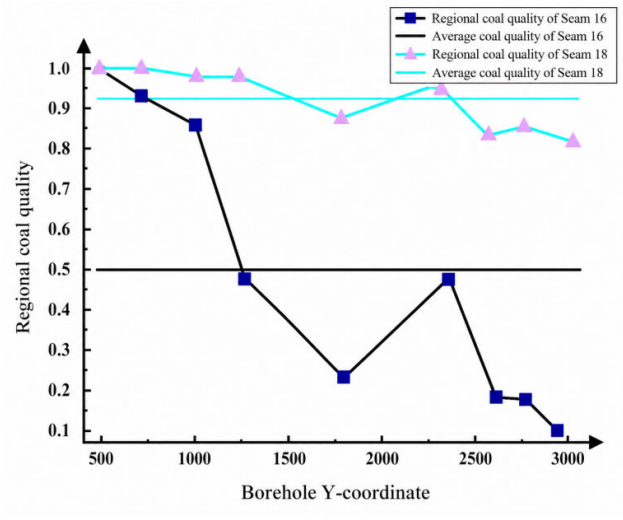


(**c**) Region [200, 300]

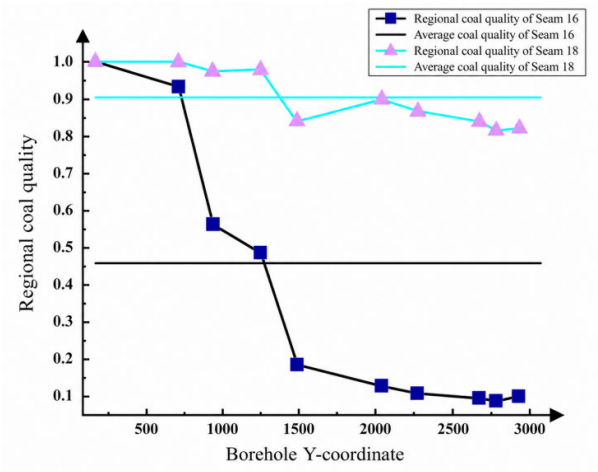


(**d**) Region [300, 400]

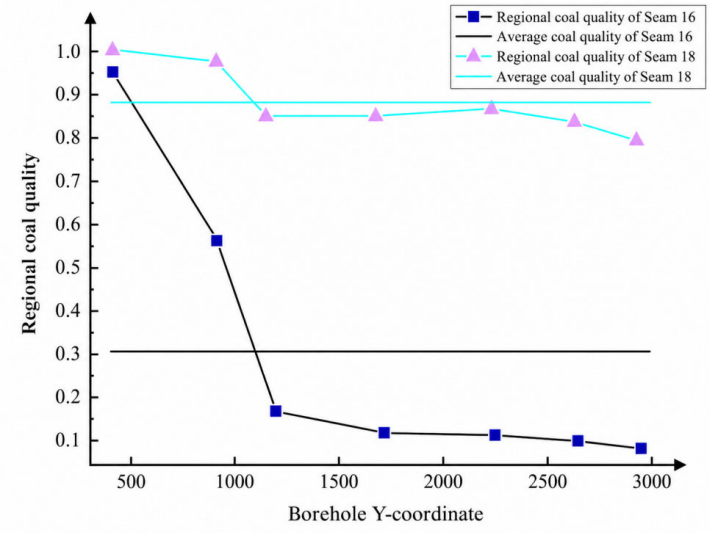
Figure 8. *Cont*.



(**e**) Region [400, 500]



(**f**) Region [500, 600]



(**g**) Region [600, 700]

Figure 8. Changes in coal quality in different regions.

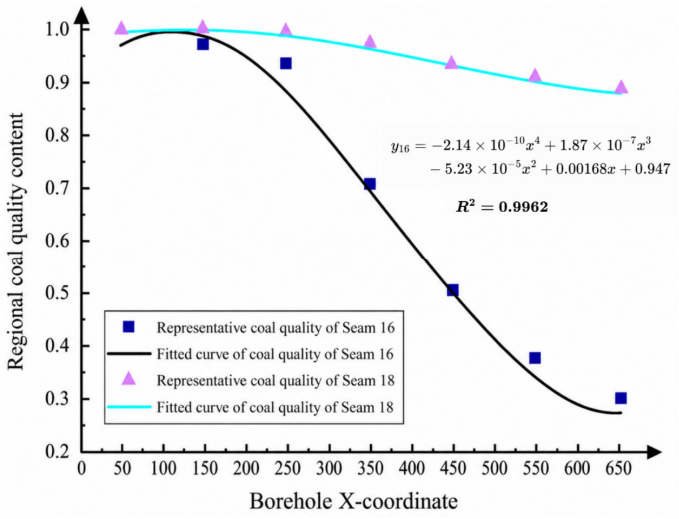


Figure 9. Overall change in coal quality in the study area.

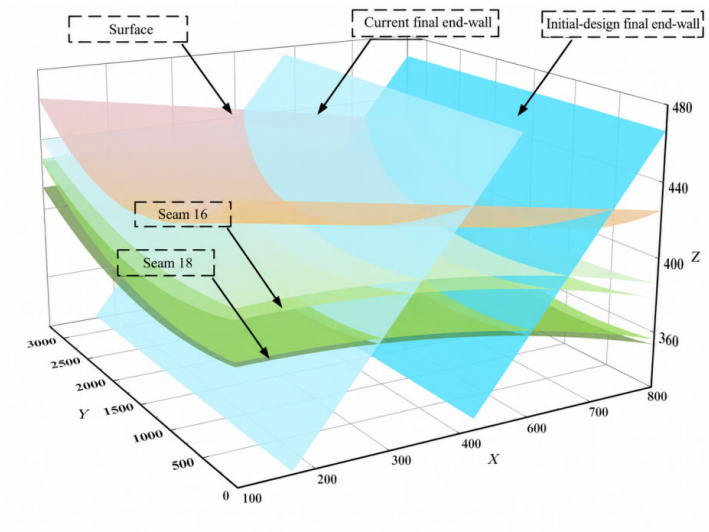


Figure 10. Mining model.

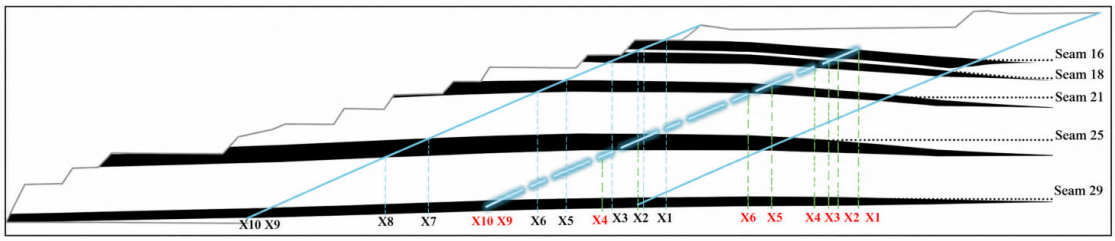


Figure 11. Coordinates of the mining locations in the study area.

Taking the overburden stripping above the No. 16 coal seam and the mining of the No. 16 coal seam as a typical calculation example, the formula for calculating the topsoil stripping volume varying with the mining advance distance, Δx, is given as follows:

$$V_{bt} = 0.1101\Delta x^3 - 28.3009\Delta x^2 + 37901.6864\Delta x \quad (8)$$

The mining volume of the No. 16 coal seam is calculated as follows:

$$V_{16} = \int_0^{3303} \int_{x_2}^{x_2'} (4.6945 + 3.7e^{-3}x + 6.3e^{-3}y - 1.4034e^{-6}y^2)dx\,dy$$
$$x_2' = x_2 + \Delta x; \quad (9)$$
$$x_2 = \frac{\sqrt{8143y^2 - 1.95e^7 y + 791132531250}}{250\sqrt{10}} - \frac{4171}{2}$$

The mining volume of the No. 16 coal seam varying with the mining advance distance, Δx, is defined by the following formula:

$$V_{16} = 6.1106\Delta x^2 + 38272.8923\Delta x \quad (10)$$

Considering the fluctuating coal quality of the No. 16 and No. 18 coal seams, the coal bulk density and coal quality correction coefficient are incorporated into the economic calculation model. After systematic sorting and derivation, the positive economic benefit generated by mining the No. 16 coal seam at the mining advance distance of Δx is expressed as follows:

$$p_{16} = \int_0^{3303} \int_{x_2}^{x_2'} f(x,y)g(y)dx\,dy$$
$$x_2' = x_2 + \Delta x;$$
$$x_2 = \frac{\sqrt{8143y^2 - 1.95e^7 y + 791132531250}}{250\sqrt{10}} - \frac{4171}{2} \quad (11)$$
$$f(x,y) = \gamma \cdot p_c \cdot (4.6945 + 3.7e^{-3}x + 6.3e^{-3}y - 1.4034e^{-6}y^2)$$
$$g(x) = 9.6389e^{-9}x^3 - 1.0894e^{-5}x^2 + 2.06e^{-3}x + 0.8893$$

Simplified as follows:

$$p_{16} = \gamma p_c (2.3560e^{-8}\Delta x^5 + 9.6953e^{-3}\Delta x^4 + 1.1751e^{-2}\Delta x^3 - 34.3203\Delta x^2 + 20152.3006\Delta x) \quad (12)$$

where γ denotes the coal bulk density, and pc represents the pithead coal price.

The multiple integral method is further applied to derive the volume integral formulas for the underlying coal seams and rock strata in sequence, and the detailed derivation processes are not repeated herein.

3.3. Construction of Mining Net Profit

3.3.1. Mining Net Profit Under Current Coal Prices

Based on the derived volume of stripped overburden and mined coal quantity at different mining positions in the study area, a mathematical model characterizing the relationship between total mining profit and mining advance distance is established in this section. In this study, the mining process is defined to terminate once coal resources are transported to the mine pithead. The commercial coal product in the research area is defined as blended coal, with a coal yield of 95.793% and a coal bulk density of 1.34 t/m^3.

To ensure the scientific rationality and engineering practicality of the established net profit model, all cost parameters adopted in the model are comprehensively calculated based on the actual engineering settlement statements and mine financial statistical data of the Dananhu No. 2 Open-Pit Coal Mine in the previous production year [25,26]. In conventional open-pit coal production, the total production cost mainly originates from four standard core operational procedures, including drilling and blasting, loading and excavation, transportation, and dumping. Combined with the local engineering consumption quota and actual equipment energy consumption of the mining area, the statistical average

values of various operational costs are adopted as the input parameters of the economic model, and the detailed parameter statistics are listed in Table 2.

Table 2. Main sources and costs of open-pit mines.

Cost Source		Average Cost
Drilling and blasting	Coal mining Stripping	8.51 yuan/t 13.97 yuan/m^3
Excavation and loading	Coal mining Stripping	5.89 yuan/t 9.98 yuan/m^3
Transportation	Coal Rock	11.57 yuan/t 15.34 yuan/m^3
Waste dumping		7.31 yuan/m^3
Total coal cost		25.97 yuan/t

After systematic conversion and calculation, the comprehensive coal mining cost (Bc) in the study area is determined as 25.97 yuan per ton, the comprehensive rock stripping cost (Bb) is 46.6 yuan per cubic meter, and the tax-excluded price of blended coal is 108.6 yuan per ton. All parameters are derived from field-measured engineering data, which effectively guarantee the reliability and accuracy of the subsequent net profit calculation and optimization results.

Simplified to the following:

$$\begin{aligned} \mathrm{Max}P = {} & p_{16} + p_{18} + \gamma \cdot b_c(V_{21} + V_{25} + V_{29}) \\ & - B_b(V_{bt} + V_{16\sim18} + V_{18\sim21} + V_{21\sim25} + V_{25\sim29}) \\ & - \gamma \cdot B_c(V_{16} + V_{18} + V_{21} + V_{25} + V_{29}) \\ s.t. \quad & 0 \le \Delta x \le 240(\mathrm{m}) \end{aligned} \tag{13}$$

Δx represents the adjustment range of the open-pit boundary expansion distance, which forms a complete closed optimization model without missing constraints. On the basis of the above parameter calibration and model derivation, the variation curve of the mining net profit with the mining advance distance is obtained, as shown in Figure 12.

Based on the established mining advance rate model correlated with the profit and coal quality, the maximum net profit of the mine reaches 676.608 million yuan when the on-site mining advance distance is 193 m during the exploitation of the overlaid coal seams in the southern end slope of the first mining panel. Nevertheless, solely adopting 193 m as the optimal mining advance distance is unreasonable and insufficient. Affected by the coal fire zone, the southern end slope suffers from coal quality degradation and deterioration of rock mechanical parameters, where intact rock masses are transformed into burnt rocks under long-term high-temperature baking effects [27,28]. Excessive mining will cause extensive exposure of burnt rock masses and further induce slope instability, which is technically infeasible. Therefore, a slope stability analysis considering the deterioration of mechanical parameters is incorporated into the optimization framework to determine the comprehensive optimal mining advance distance by coupling economic and safety constraints.

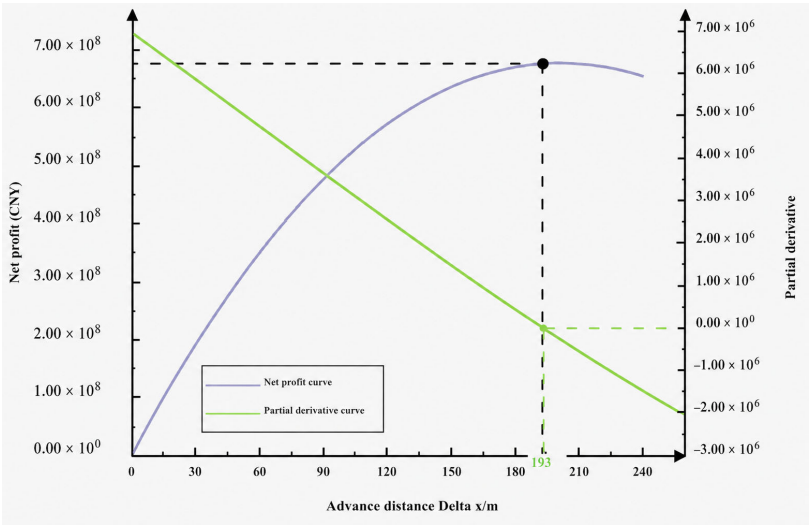


Figure 12. Net profit curve.

3.3.2. Sensitivity Analysis of Net Profit Under Coal Price Fluctuations

To overcome the applicability limitation of the net profit caused by fixed coal price parameters, this subsection conducts a sensitivity analysis under variable coal price scenarios. All benchmark parameters in Table 2 (including coal yield, bulk density, stripping cost, and coal mining cost) remain unchanged, and the effects of coal price fluctuations on the net profit curve, optimal advance distance, and maximum net profit are quantitatively investigated.

Let p denote the benchmark tax-excluded coal price and δ represent the coal price disturbance coefficient. The variable coal price scenarios can be defined as follows:

$$p = p_0(1+\delta) \tag{14}$$

where p = 108.6 yuan/t, and the disturbance coefficient, δ, is set within the range of {−30%, −20%, −15%, −10%, −5%, 0, 5%, 10%, 15%, 20%, 30%}. The variation law of the net profit with the mining advance distance, Δx, under the benchmark coal price, p, is illustrated in Figure 12. The benchmark optimal advance distance and the corresponding maximum net profit are determined as Δx = 193 m and P = 676.608 million yuan, respectively. To rapidly reconstruct the net profit curves and solve the optimal advance distance under various coal price disturbance scenarios, a quadratic surrogate model is established based on the benchmark curve in Figure 12:

To extract the baseline curve parameters from the standard coal price case, set the fixed baseline coal price at p_0 = 108.6 yuan/t, the comprehensive mining cost at Bc = 25.97 yuan/t, the baseline optimal advance distance at Δx0 = 193 m, and the corresponding maximum net profit at Pmax,0 = 67,660.8 ten thousand yuan. Establish the baseline quadratic surrogate function at $P(\Delta x,p_0)$ = AΔx2 + B0Δx, and subject it to the following three constraints: zero profit at zero advance (P(0) = 0), extreme value at Δx0, and peak profit equals Pmax,0. Solve to obtain constant coefficients A and B0. Introduce coal price disturbance factor δ and disturbed coal price $p = p_0(1 + \delta)$. Assume net profit scales linearly with unit net income (p−Bc), then scale the linear term coefficient to derive B(p), while quadratic coefficient A remains unchanged for all price scenarios. Substitute B(p) into the baseline surrogate formula to obtain the universal net profit function applicable to the arbitrary coal price fluctuation scenario.

$$\Delta x^*(p) = \Delta x \cdot \frac{(p - B_c)}{(p_0 - B_c)} \tag{15}$$

The unconstrained optimal mining advance distance is derived by solving the extremum of Equation (15). Considering the practical mining constraint of the advance distance within the range of $0 \leq \Delta x \geq 240$ m, the constrained optimal advance distance is finally determined as follows:

$$\Delta x^*(p) = \min\left(\Delta x \cdot \frac{(p - B_c)}{(p_0 - B_c)}, 240\right) \quad (16)$$

The threshold coal price corresponding to the upper-bound constraint is further obtained from Equation (17), as follows:

$$p_{th} = B_c + (p_0 - B_c)\frac{240}{\Delta x_0} \approx 128.72 \quad (17)$$

When the coal price p ≥ p, the optimal mining advance distance is constrained by the upper boundary limit of Δx = 240 m. Table 3 summarizes the optimal advance distances and the corresponding maximum net profits under eleven coal price scenarios. Overall, a decline in the coal price leads to a significant reduction in both the optimal mining advance distance and maximum net profit, while an increase in the coal price promotes a larger optimal advance distance. When the coal price rises above approximately 128.72 yuan/t (an increase of about 18.5%), the optimal advance distance reaches the upper limit of 240 m, and the optimization results are dominantly controlled by the boundary constraint.

Table 3. Optimal advance rate and maximum net profit under coal price fluctuation scenarios.

Coal Price Disturbance Coefficient (δ)	Coal Price, p (yuan/t)	Optimal Mining Advance Distance, Δx* (m)	Maximum Net Profit, P_{max} (10,000 yuan)	Relative Change (vs. Baseline)
−30%	76.02	116.9	24,823.9	−63.31%
−20%	86.88	142.3	36,765.4	−45.66%
−15%	92.31	155.0	43,612.7	−35.54%
−10%	97.74	167.6	51,044.3	−24.56%
−5%	103.17	180.3	59,060.4	−12.71%
0%	108.60	193.0	67,660.8	0.00%
+5%	114.03	205.7	76,845.6	+13.57%
+10%	119.46	218.4	86,614.8	+28.01%
+15%	124.89	231.0	96,968.3	+43.32%
+20%	130.32	240.0	107,880.9	+59.44%
+30%	141.18	240.0	129,997.3	+92.13%

When the coal price p ≥ p, the optimal mining advance distance is constrained by the upper boundary limit of Δx = 240 m. Specifically, when the disturbance coefficient δ ≥ 20%, the unconstrained optimal solution of Δx* exceeds 240 m and is truncated by the upper boundary, thereby making 240 m the constrained optimal advance distance.

Figure 13 presents the family of net profit curves under various coal price disturbance scenarios. The overall profit curve shifts upward with its peak position moving rightward as the coal price increases, while an opposite variation trend is observed under coal price reduction. Figure 14 further illustrates the evolutionary characteristics of optimization indicators with fluctuating coal prices. The optimal advance distance increases approximately linearly with the rising coal price and then enters a plateau stage dominated by boundary constraints after reaching the upper limit of 240 m, while the maximum net profit exhibits a significant nonlinear growth trend with the increase in coal price.

Before the optimal advance distance touches the upper boundary constraint, it can be concluded from Equations (13) and (14) that Δx* is positively proportional to the net

unit coal profit (p−Bc), and the maximum net profit P approximately increases with the square of (p−Bc). Once the upper boundary constraint is activated, the variation law of the maximum net profit is converted to the objective function value variation under the fixed mining advance distance of Δx = 240 m.

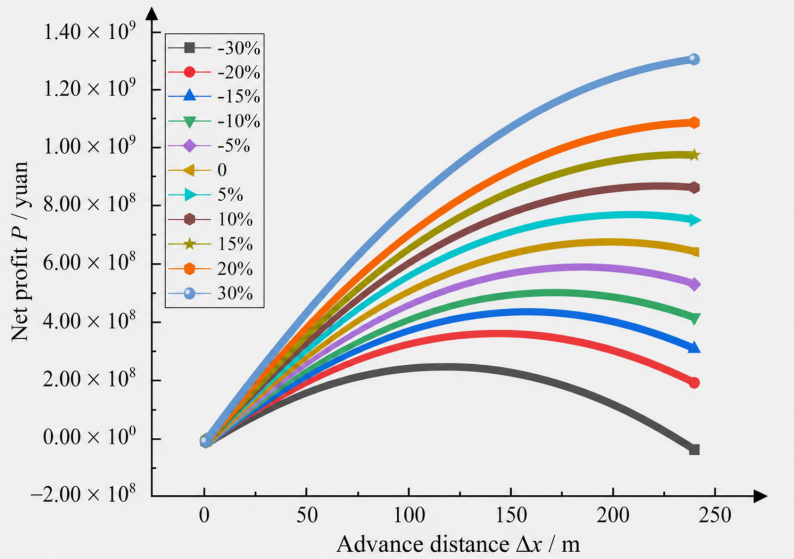


Figure 13. Net profit curve families under volatile coal prices.

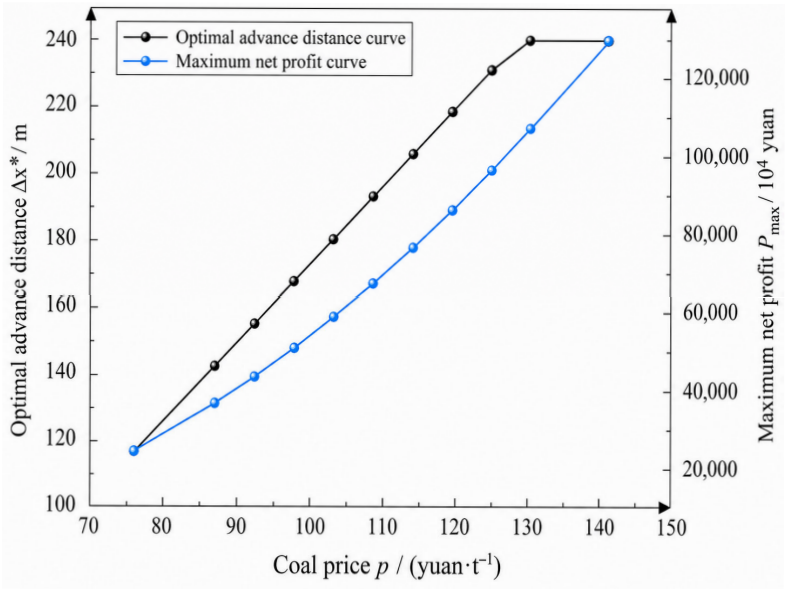


Figure 14. Curves of optimal advance rate and maximum net profit.

With parameters such as stripping and coal mining costs kept constant, coal price fluctuations significantly alter the peak position and amplitude of the net profit curve. A decline in coal price leads to a reduced optimal mining advance distance and a substantial decrease in the maximum net profit, whereas an increase in coal price promotes the expansion of the optimal advance distance. When the coal price exceeds approximately 128.72 yuan/t, the optimal advance distance reaches the upper limit of 240 m, and the optimal solution is completely controlled by the boundary constraint. The above results demonstrate that the introduction of coal price scenario analysis effectively improves the adaptability of the economic model to market fluctuations and can provide a reliable basis for the dynamic decision making of mining boundaries under different market conditions.

3.4. Slope Stability Analysis of the Study Area

3.4.1. Experimental Analysis of Mechanical Parameters of Burnt Rock

To quantitatively evaluate the slope stability of the study area affected by coal fire baking, it is essential to clarify the differences in mechanical parameters between intact rock masses and thermally altered burnt rock masses. In this study, field rock sampling and indoor mechanical tests were conducted to obtain the physical and mechanical parameter variations in rock masses under fire influence.

Burnt rock masses are characterized by extremely developed fractures, exhibiting distinct physical and mechanical properties compared with original intact rocks. Such rocks possess high water absorption capacity, poor frost resistance and poor disintegration resistance. Under the combined effects of drastic temperature variation, freeze–thaw cycles and groundwater erosion in the open-air environment, burnt rock masses are prone to rapid disintegration and spalling, which eventually leads to rock mass failure and slope deformation [29,30].

Rock specimens were processed into standard cuboid samples with a length and width of 5 cm and a height of 10 cm for rock deformation tests (Figure 15). The axial and radial deformations of specimens under longitudinal compressive loading were measured, based on which the elastic modulus and Poisson's ratio of the rock masses were calculated.



(**a**) Typical sample photograph



(**b**) 5 cm × 5 cm × 10 cm sized sample

Figure 15. Specimens.

Subsequently, uniaxial compressive tests and tensile tests were performed on the prepared rock specimens. The detailed test procedures and corresponding results are illustrated in the following Figures 16–19.

Based on the laboratory test results, combined with field investigations on joint fracture development, weathering degree, and structural plane occurrence, parameter reduction (equivalent conversion) was conducted on the mechanical parameters of the intact rock. The equivalent mechanical parameters of the end-slope rock mass adopted for numerical simulation are summarized in Table 4.

Significant differences exist between the mechanical parameters of the laboratory intact rock specimens and in situ rock masses. In this study, the equivalent rock mass

parameters are determined by combining laboratory test data with field structural plane reduction correction. Furthermore, the rationality of the calibrated parameters is verified by analyzing the displacement response and plastic zone distribution obtained from numerical calculations, which reduces the deviation between the simulation results and the actual engineering conditions.



Figure 16. Determination of the uniaxial compressive strength of the rock.

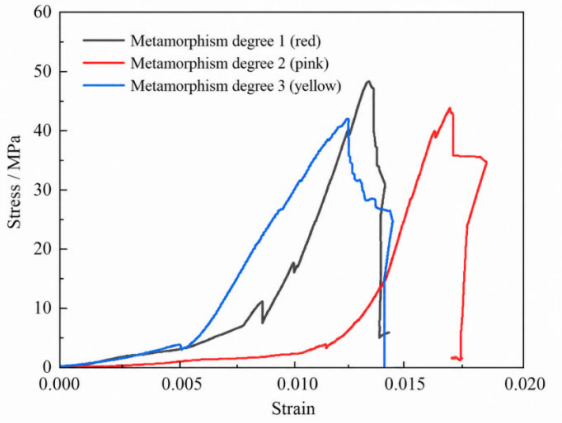
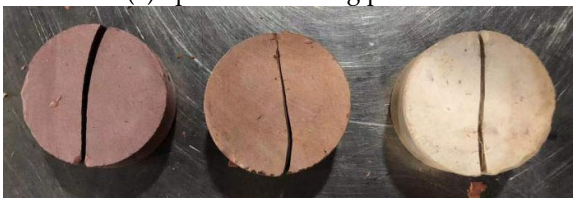


Figure 17. Measured results of the uniaxial compression of the rocks.



(**a**) Specimen loading process



(**b**) Specimen loading completion

Figure 18. Determination of the uniaxial tensile strength of the rocks.

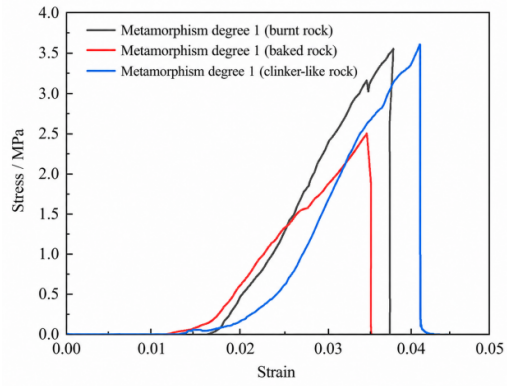


Figure 19. Measured results of uniaxial tensile strength of rocks.

Table 4. Equivalent mechanical parameters of the rock mass at the end slope.

Lithology	Density (g·cm^{-3})	Cohesion (kPa)	Internal Friction Angle (°)	Elastic Modulus (MPa)	Poisson's Ratio
Waste dump material	1.70	25	22.00	373	0.273
Interbedded sandstone and mudstone	2.27	253	24.23	451	0.248
Mudstone	1.92	120	18.01	464	0.357
Fine sandstone	1.88	1560	37.69	702	0.272
Sandstone	2.05	984	34.75	878	0.349
Burnt rock	2.06	50	23.22	524	0.210
Coal	1.34	150	16.80	231	0.260

3.4.2. Three-Dimensional Slope Stability Verification

Model Establishment and Boundary Conditions

The southern composite slope of the first mining panel of the Dananhu No. 2 Open-Pit Coal Mine consists of multiple coal and rock strata, leading to substantial complexity in direct model establishment using FLAC3D. Therefore, Rhino 6.0 is adopted to construct the slope geometric model, and the Griddle plug-in is utilized for mesh generation. The finalized mesh model is subsequently imported into FLAC3D for numerical simulation and calculation.

To guarantee the accuracy of the numerical simulation, typical slope profiles are selected as research objects. Corresponding numerical models of the southern end slope, internal dump, and composite slope before and after optimization are established. This modeling scheme aims to reveal the evolutionary mechanism of slope instability and verify the reliability and accuracy of the two-dimensional slope stability analysis results. The established numerical model is presented in the Figure 20.

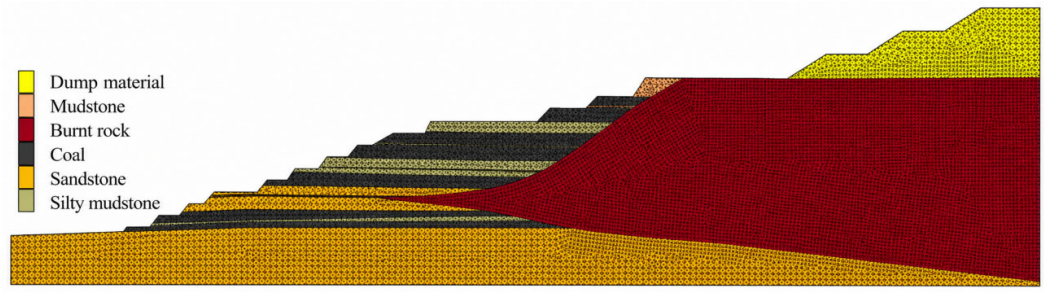


Figure 20. Typical profile of the Nanbang slope.

To reduce the computational cost of the FLAC3D numerical simulation, the width of the numerical model along the Y-direction is set to 1 m. To eliminate the boundary effect of the model, horizontal displacement constraints are applied to the surrounding boundaries of the model, and full fixed constraints are assigned to the model bottom. The top surface and slope surface are set as free boundaries. Gravity stress is applied along the Z-direction of the model, while horizontal in situ stress is not considered. The model is loaded under self-weight conditions, and the Mohr–Coulomb elastoplastic constitutive model is adopted for all rock and coal materials in the numerical model.

3.5. Analysis of Numerical Simulation Results of Slope Stability

Horizontal displacement constitutes the dominant deformation mode of slope movement. Figure 21 displays the horizontal displacement nephogram of the southern end slope. It can be observed that the horizontal displacement generally decreases gradually from the top to the bottom of the slope and radiates outward from a specific central zone. The maximum displacement zone is mainly concentrated in silty mudstone, coal seams and burnt rock areas, where the peak horizontal displacement occurs.

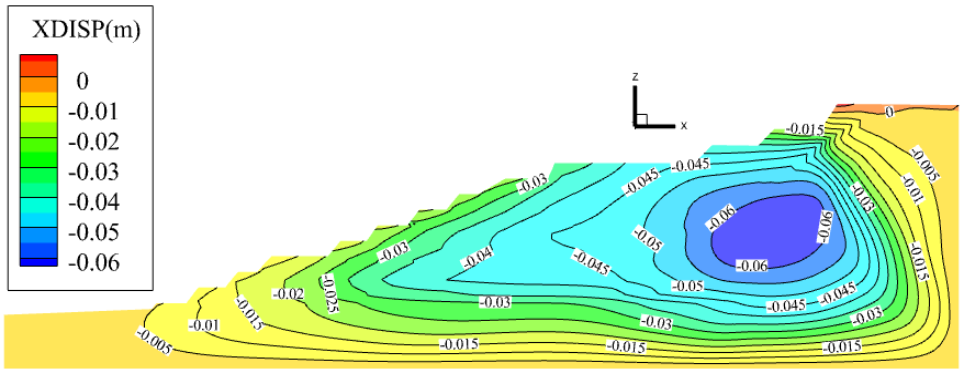


Figure 21. Horizontal displacement contour of the south slope.

This deformation characteristic is primarily attributed to shear failure between rock strata induced by slope excavation and unloading, which leads to progressive relaxation of the slope mass structure. Under the combined action of self-weight stress and horizontal tectonic stress, the southern end slope gradually creeps and deforms toward the free face. Furthermore, burnt rock masses are characterized by low rock strength and poor shear resistance, making them susceptible to significant compressive deformation. Accordingly, the maximum displacement center is ultimately located within the coal fire-affected burnt rock zone.

The penetration of the plastic zone is an essential prerequisite for slope failure. Figure 22 illustrates the plastic zone distribution nephogram of the southern end slope. It can be seen that the plastic zone of the southern end slope is mainly distributed in two regions, namely, the coal fire zone and glutenite stratum. A large-scale plastic zone develops within the fire-affected burnt rock zone due to the low strength of thermally altered rock masses, which readily generates compression-induced tensile fracture surfaces under compressive loading. Under the long-term action of self-weight stress, continuous stress accumulation occurs in the rock locking segments between compression-induced tensile fractures and unloading cracks, eventually triggering brittle shear failure of the rock mass.

After the redesign of the southern end slope, the plastic zone is predominantly concentrated within the burnt rock zone. The evolutionary characteristics of the plastic zone indicate that the increase in the slope angle promotes the penetration trend of the plastic zone, forming a continuous shear failure zone. Stress differentiation easily induces tensile

cracks at the slope crest, whereas the slope surface remains in a relatively stable state throughout the deformation process.

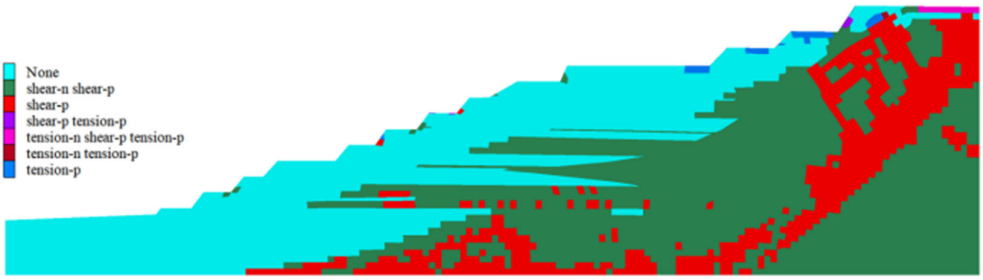


Figure 22. Distribution of the contour of the plastic zone in the south slope.

Tensile failure mainly occurs at the slope crest and slope surface. This phenomenon is caused by differential unloading and rebound deformation of rock masses induced by slope excavation. The tangential stress at the slope crest and radial stress on the slope surface are converted into tensile stress, forming a tensile stress concentration zone. The resultant stress redistribution and stress concentration effects ultimately lead to dominant tensile failure in the slope crest area.

Figure 23 shows the maximum unbalanced stress curve of the southern end slope. The calculated maximum unbalanced force ratio of the numerical system is lower than the default convergence criterion of 10. The maximum unbalanced stress curve presents a continuous convergent trend, and the internal stress of the model gradually reaches a balanced state, indicating that the southern end-slope model maintains a stable plastic rheological state.

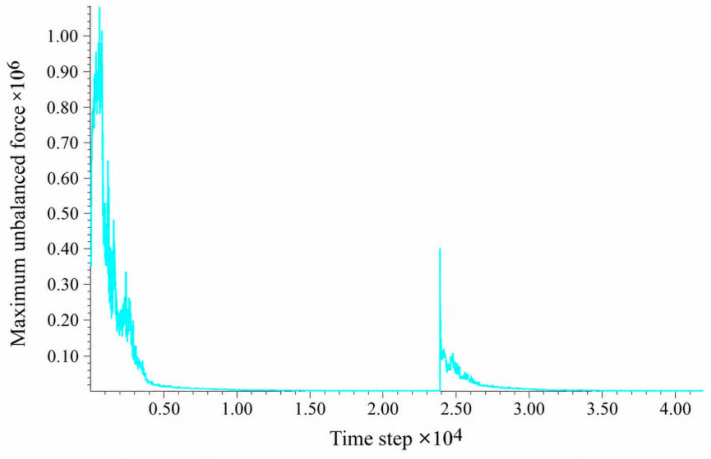


Figure 23. Diagram of the unbalanced stress curve of the south slope.

Landslide is the most common deformation and failure mode of slope rock masses. Figure 24 presents the nephogram of the maximum shear strain increment of the southern end slope automatically calculated via the strength reduction method. An obvious potential sliding zone can be clearly observed in the southern end slope, where the sliding surface cuts out along the No. 29 coal seam at the +415 m horizontal level. With the continuous increase in mining depth of the southern end slope, the rock mass is affected by self-weight stress and excavation unloading. The tangential stress at the slope toe increases significantly, while the radial stress decreases sharply and may even transform into tensile stress under extreme conditions. The resulting high stress difference generates intense shear stress at the slope toe. Therefore, the maximum shear strain increment zones of the southern end

slope before and after optimization are both concentrated in the silty mudstone and No. 29 coal seam at the slope toe.

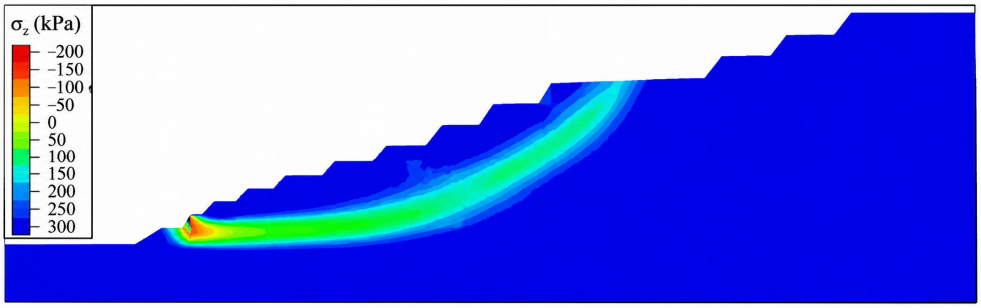


Figure 24. Max shear strain increment contour of the south slope.

The potential instability mode of the optimized southern end slope is identified as bedding shear sliding. According to the calculation results of the strength reduction method, the stability factor of the southern end slope is 1.27, which is consistent with the judgment of the potential sliding failure mode and verifies the rationality of the two-dimensional stability analysis results of the southern end slope. The safety factor (FoS) calculated via the strength reduction method is 1.27, which falls within the acceptable stability threshold.

3.6. Optimization Results of Mining Boundary

In this study, a comprehensive optimization of the mining boundary for the coal fire zone on the southern end slope of the first mining panel in the Dananhu No. 2 Open-Pit Coal Mine is performed, taking the maximum economic benefit as the objective function and slope stability as the pre-safety constraint. The core parameters and comparative results of the optimization scheme obtained via the model calculation and numerical simulation are presented in the following.

3.7. Comprehensive Optimized Boundary and Core Indicators

Based on the established coal quality–profit multiple integral model, under the benchmark coal price of p = 108.6 yuan/t, the net profit curve reaches its peak when the mining advance distance, Δx, of the southern end slope is 193 m, with the maximum total mining net profit of 676.608 million yuan achieved for the mining system.

Under this economically optimal advance distance, a three-dimensional numerical simulation and strength reduction calculation are conducted for the composite end slope. The results show that although a certain penetration trend of the plastic zone occurs in the coal fire zone and glutenite area at the advance distance of 193 m, the overall maximum unbalanced force of the model converges steadily. The calculated three-dimensional slope stability factor, Fs, of the southern end slope is 1.27, which meets the safety specification requirements for open-pit slope engineering.

In terms of spatial morphology, when the optimal mining advance distance is fixed at 193 m, the surface boundary of the southern end slope in the first mining panel retreats inward by 47 m compared with the original full-boundary mining design scheme. The planar and profile variations in the optimized deep mining boundary of the southern end slope are illustrated in Figure 25.

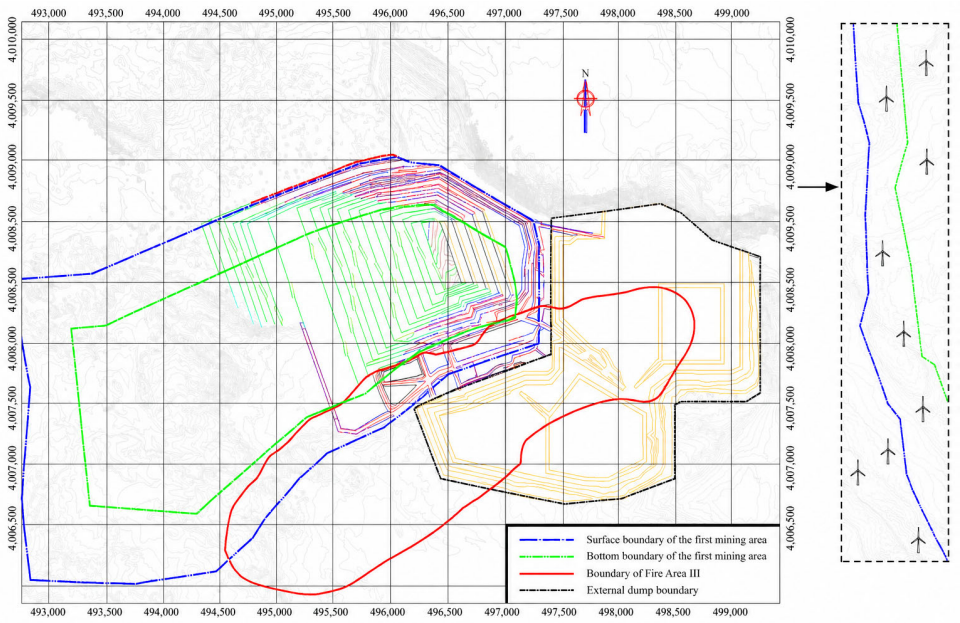


Figure 25. Optimized deep boundary diagram of the southern end.

3.8. Benefit Comparison of Mining Schemes Before and After Optimization

To quantitatively and intuitively evaluate the practical engineering effectiveness of the proposed mining boundary optimization model, three typical mining decision schemes for the coal fire zone on the southern end slope of the first mining panel are selected for the calculation and comparison of key evaluation indicators.

Scheme A (current status with no mining of overlaid coal resources): to completely avoid the risks of coal quality degradation in the coal fire zone and landslide failure of burnt rock masses, an in situ retention strategy is adopted with a mining advance distance of $\Delta x = 0$ m.

Scheme B (original full-boundary mining scheme): neglecting the spatial variability of coal quality deterioration and rock mass mechanical weakening, the full recovery of the No. 16 and No. 18 coal seams on the southern end slope is implemented in strict accordance with the original design, with the mining advance distance reaching the ultimate boundary of $\Delta x = 240$ m.

Scheme C (proposed optimized scheme in this study): the recommended mining scheme determined by the comprehensive optimization model established in this study, with an optimal mining advance distance of $\Delta x = 193$ m.

The geometric boundary parameters of the three aforementioned schemes are imported into the benefit evaluation model and safety verification model constructed in this study. The comprehensive quantitative comparison results are summarized in Table 5.

As shown in the statistical results in Table 5, Scheme A yields zero economic profit and causes severe resource stagnation. Although Scheme B maximizes the mining advance distance, it reduces the slope stability factor below the safety threshold ($Fs < 1.0$) and results in a serious decline in overall economic benefits due to the increased proportion of low-quality coal. In contrast, Scheme C fully satisfies the safety constraint with a slope stability factor of 1.27. It not only achieves the maximum net profit of 676.608 million yuan but also reduces the surface mining boundary by 47 m, realizing the dual optimization of economic and safety indicators at the quantitative level.

Table 5. Comparison of the comprehensive benefits of southern highwall fire mining area exploitation plans before and after optimization.

Comparison Index	Scheme A (Retained and Unmined Under Current Condition)	Scheme B (Original Full Limit Mining)	Scheme C (Optimized Scheme in This Study)
Mining advance distance Δx (m)	0	240	193
Surface boundary retraction distance (m)	147	0	47
Slope stability factor (Fs)	>1.27	<1.0 (High risk of bedding sliding)	1.27
Calorific value characteristic of mined coal	No coal mined	Extremely low (mixed with massive severely combusted inferior coal)	Relatively high (avoiding the boundary of severe spontaneous combustion zone)
Total net profit (10^4 yuan)	0	Profit decline	67,660.8

4. Discussion

4.1. Engineering Feasibility and Mechanism Analysis of Optimized Mining Boundary

Based on the multi-factor coupled optimization framework integrating coal quality variation, slope stability, and economic benefit, the optimal mining advance distance of 193 m is determined for the coal fire zone on the southern end slope of the first mining panel. Different from traditional decision-making methods relying merely on the stripping-to-ore ratio or empirical judgment, the proposed optimization result is strongly supported by systematic engineering mechanism analysis.

From the perspective of economic efficiency, coal spontaneous combustion in fire-affected coal seams leads to nonlinear spatial degradation of coal calorific value. As verified by the aforementioned results, advancing the mining working face to the ultimate boundary of 240 m (Scheme B) will trigger severe economic cost inversion. The deep No. 16 and No. 18 coal seams suffer the most severe spontaneous combustion damage, and the pithead sales price of the thermally degraded coal fails to cover the comprehensive costs of drilling and blasting, excavation, and transportation. Excessive mining will instead erode the accumulated economic benefits. Significant disparities in calorific value attenuation are observed between No. 16 and No. 18 coal seams. The No. 18 seam is closer to the central spontaneous combustion zone with shallow burial depth and high interlayer fracture permeability, leading to sufficient oxygen infiltration and severe thermal deterioration of coal quality. In contrast, the No. 16 seam lies far from the fire source and is covered by thick low-permeability overburden, which restricts heat and oxygen transfer and weakens coal quality loss. The 193 m advance distance is the multi-objective equilibrium point of economic profit, coal quality loss and slope stability. When the boundary is less than 193 m, massive coal resources are abandoned and total profit declines; if the boundary exceeds 193 m, mining enters heavily burnt zones with sharply reduced unit coal value, while the slope safety factor drops below the standard threshold. Geologically, this boundary avoids the highly fractured thermal damage zone of the end slope, effectively reducing landslide risks while balancing resource recovery, which provides a reliable geological basis for safe and low-disturbance exploitation of fire-affected open-pit highwalls.

In terms of the slope safety mechanism, long-term high-temperature baking in the coal fire zone transforms the surrounding intact rock masses into burnt rock with extremely low shear strength. If the mining advance distance reaches 240 m, the large-scale exposure of

burnt rock masses will deprive the slope toe of effective support, easily inducing bedding sliding failure along weak interlayers (silty mudstone or the floor of the No. 29 coal seam). In this study, the slope stability factor (Fs $\geq$ 1.2) is set as the mandatory pre-constraint for mining boundary decision making. The optimized boundary with a 193 m advance distance realizes a 47 m inward shrinkage of the surface boundary, which retains sufficient safety rock and coal pillars to stabilize the slope toe. Meanwhile, no continuous shear failure channel is formed in the plastic zone of the southern end slope, fundamentally guaranteeing slope stability.

4.2. Dynamic Response of Optimized Mining Boundary to Coal Price Fluctuations

The proposed mining boundary optimization model achieves a reliable application performance under the benchmark coal price of p = 108.6 yuan/t. Nevertheless, fluctuations in coal market prices directly alter the profile of the net profit function, thereby inducing dynamic variation in the optimal mining boundary. To verify the universality and robustness of the established model, a dynamic sensitivity analysis is conducted under various coal price disturbance scenarios [31]. From the perspective of an economic assessment, the sensitivity analysis carried out in this study only regards coal price as the variable parameter, while excavation cost, stripping cost, transportation cost and other mining production expenditures are fixed as constant values. This single-variable sensitivity scheme is simplified to focus on the response law of optimal mining boundary under coal price fluctuation, which is conducive to highlighting the core research theme of this paper. Nevertheless, actual open-pit mining economics involves multi-source cost uncertainties, and the simultaneous variation in various production costs will jointly affect the net profit and optimal advance distance. Therefore, the economic sensitivity results derived in this study are only applicable to a scenario where all mining costs remain stable.

With all cost parameters including stripping and coal mining costs kept constant, coal price fluctuations significantly affect mining decision making, as demonstrated in Table 3 and Figures 13 and 14.

Boundary contraction effect during coal price decline: A decrease in coal price advances the occurrence of cost inversion for low-quality coal mining, forcing the optimal mining advance distance to shrink inward sharply. Specifically, when the coal price drops by 30%, the optimal advance distance decreases to 116.9 m, and the maximum net profit is drastically reduced to 248.239 million yuan. This indicates that a conservative mining strategy should be adopted during market downturns, and the coverage of reserved coal resources needs to be expanded to avoid economic losses.

Boundary expansion and constraint limitation during coal price rise: On the contrary, a substantial increase in coal price restores the economic value of slightly spontaneous combusted coal seams, promoting the outward expansion of the optimal mining advance distance. However, such expansion is not unlimited. The calculation results show that when the coal price rises to approximately 128.72 yuan/t (an increase of 18.5%), the optimal advance distance reaches the upper threshold of spatial geometry and slope safety constraint (240 m). Afterwards, even with continuous coal price growth, the mining boundary is locked at 240 m due to the strict slope safety constraint, and the optimal solution is completely dominated by boundary conditions.

This study develops a static mining boundary optimization model for fire-affected open-pit highwalls by coupling coal quality degradation, static slope stability and coal price volatility. The thermally altered rock mechanical parameters used in the FLAC3D numerical calculations are sourced from short-term laboratory tests, which cannot account for long-term weathering-induced progressive deterioration and creep damage of rock masses. Persistent weathering continuously degrades rock mass strength and lowers the

critical stability threshold of pit slopes. Additionally, the numerical model neglects boundary conditions corresponding to rainfall infiltration and seasonal groundwater fluctuations. Transient pore water pressure arising from such hydrological processes reduces the shear strength of fractured burnt rock and poses potential risks of shallow slope sliding. Moreover, the optimized scheme only characterizes static slope equilibrium under invariant hydrogeological conditions within a single mining stage, and fails to capture the long-term geotechnical evolution of fire-affected highwalls across the full mine service life. Consequently, the optimal mining advance distance determined in this work is only applicable to short-term static stability evaluation under the present geological settings. In summary, the proposed comprehensive optimization decision model breaks the extreme mining dilemma of full resource abandonment or complete exploitation in coal fire zones. With excellent dynamic adaptability, it can provide a scientific quantitative tool for the medium- and long-term mining planning of open-pit mines under complex geological conditions in Northwest China.

4.3. Limitations of the Present Study

The static coupling optimization framework for mining advance boundaries of fire-affected open-pit highwalls proposed in this work incorporates several simplification assumptions that constrain its general applicability. Geotechnical simulations adopt mechanical parameters of thermally altered rock derived from short-term laboratory tests, neglecting long-term weathering-induced progressive deterioration, creep deformation, rainfall infiltration and seasonal groundwater fluctuations. The optimized boundary merely reflects static slope equilibrium under fixed hydrogeological conditions at a single mining stage and fails to capture long-term geotechnical evolution across the full mine service life. In terms of economic evaluation, a static net profit calculation approach is adopted without accounting for the time value of capital required for standard NPV analysis. Furthermore, the sensitivity analysis only takes coal price as the variable parameter while excavation, stripping and transportation costs are held constant, ignoring multi-source cost fluctuations in practical open-pit mining. Accordingly, the derived optimal advance distance is only valid for short-term static assessment under the geological and cost conditions defined in this study. Future research will integrate creep constitutive models, variable seepage boundaries and multi-factor variable cost modules to establish a long-term dynamic boundary optimization framework coupled with hydrological weathering effects and multi-dimensional economic uncertainties.

5. Conclusions

Targeting the engineering challenges of coal quality degradation, resource retention, and slope safety constraints caused by coal spontaneous combustion in the coal fire zone on the southern end slope of the first mining panel of the Dananhu No. 2 Open-Pit Coal Mine, this study constructs a loss-reducing mining optimization model with the objective of maximizing mining net profit. Through three-dimensional geometric modeling of coal seams and the refined calculation of mineral resources and economic benefits, the net profit response law under different mining advance distances is obtained. On the basis of the economically optimal solution, three-dimensional numerical simulation and the strength reduction method are adopted for slope safety verification, forming a complete mining boundary determination framework of “economic optimization + safety verification”. Furthermore, coal price fluctuation scenarios are established for sensitivity analysis to quantify the influence of market changes on the optimal advance distance and maximum net profit, providing a reliable quantitative basis for dynamic decision making and low-disturbance mining in coal fire zones. This method is applicable to open-pit coal mines

with shallow coal spontaneous combustion zones characterized by gradual coal quality deterioration and thermally weakened surrounding rock. The model can be transferred to other similar mines on the premise that complete borehole sampling data of calorific value, measured mechanical parameters of burnt rock, and stable 3D terrain modeling conditions are available. The main conclusions are summarized as follows:

1. Aiming at the coexisting engineering problems of severe coal quality attenuation and mechanical parameter weakening of burnt rock in open-pit coal fire zones, this study abandons the traditional static stripping-to-ore ratio evaluation method and establishes a comprehensive mining boundary optimization model that takes net profit maximization as the objective and slope stability factor as the safety constraint. The proposed model realizes the transformation of coal fire zone mining decision making from empirical qualitative avoidance to scientific quantitative optimization.
2. Under the benchmark coal price condition of the study mine, the optimal mining advance distance of the southern end slope is determined as 193 m. To test the robustness of the optimal 193 m advance distance, we conducted parameter disturbance analysis for four major parameters within actual engineering ranges. The optimal boundary is most sensitive to coal price, moderately sensitive to stripping cost, and slightly affected by rock mechanical parameters and recovery rate. The optimal distance only fluctuates in a small range when parameters change within normal engineering intervals, demonstrating the stable and reliable performance of the 193 m optimization scheme. This optimized boundary effectively avoids the cost inversion risk induced by deep severely combusted coal seams and achieves a maximum global net profit of 676.608 million yuan. Meanwhile, the corresponding slope stability factor reaches 1.27, which fully meets the industry safety specifications. Compared with the original full-boundary mining scheme, the optimized surface boundary retreats inward by 47 m, which guarantees engineering safety and economic benefits while significantly reducing surface ecological disturbance.
3. Based on the strong coupling between coal price and optimal advance distance, we analyzed dynamic boundary adjustment strategies corresponding to high, medium and low coal price cycles and explained that mine decision-makers can dynamically adjust the exploitation range year by year according to market price trends instead of applying a fixed static boundary throughout mining periods, Coal price fluctuations exert a significant dynamic control effect on the optimal mining boundary. A coal price decline forces the inward contraction of the optimal advance distance and greatly reduces mining net profits. In contrast, coal price growth promotes boundary expansion. However, when the coal price exceeds the threshold of approximately 128.7 yuan/t, the optimal boundary is constrained by the upper limits of spatial geometry and slope safety and stops outward expansion. This revealed dynamic market constraint mechanism provides a prospective theoretical basis for medium- and long-term mining decision making of mining enterprises under different market cycles.

Author Contributions: Conceptualization, Y.L. and Z.S.; methodology, Y.L.; software, Y.L.; validation, Y.L. and Z.S.; formal analysis, Y.W.; investigation, K.Z.; resources, Z.S.; data curation, Y.L.; writing—original draft preparation, Y.L.; writing—review and editing, Y.L.; visualization, Y.L.; supervision, Y.L.; project administration, Y.L.; funding acquisition, Z.S. All authors have read and agreed to the published version of the manuscript.

Funding: This research was funded by the National Natural Science Foundation of China (51474119), the Liaoning Technical University of Engineering and Technology Ordos Research Institute campus-site science and technology cooperation cultivation project (YJY-XD-2023-027), and the Liaoning

Technical University of Engineering and Technology Collaborative Innovation Center for Mining Major Disaster Prevention and Environmental Restoration Open Project (CXZX-2024-01).

Institutional Review Board Statement: Not applicable.

Informed Consent Statement: Not applicable.

Data Availability Statement: The data used to support the findings of this study are available from the corresponding author upon request.

Acknowledgments: The authors would like to thank the School of Mining Engineering and the School of Environment for their support for this research work. The authors would also like to thank all the reviewers who participated in the review process. No generative-AI tools were used during the preparation of this manuscript.

Conflicts of Interest: Author Kun Zhang was employed by the company China Coal Pingshuo Group Co., Ltd., Shuozhou, China. The remaining authors declare that the research was conducted in the absence of any commercial or financial relationships that could be construed as a potential conflict of interest.

References

1. Song, Z.L.; Guo, S.P.; Hui, J.; Jia, Z.Z. Dust emission law and dust suppression technology of working face in burnt rocks of open-pit coal mine. *J. Liaoning Tech. Univ. (Nat. Sci. Ed.)* **2021**, *40*, 401–408.
2. Wang, H. Technologies for water hazard prevention and control in burnt rock aquifers within concealed burnt areas. *Coal Geol. Explor.* **2024**, *52*, 88–97.
3. Jin, X.Y.; Li, Y.; Yu, L.; Li, M.N.; Cao, X.H.; Wang, N.; Guo, M.H.; Xia, X.; Ren, Y.Q. Construction and Application of Green and Low-Carbon Evaluation Indicators in Coal Mining Areas. *Coal Sci. Technol.* **2024**, *52*, 131–142.
4. Xu, X.; Gu, X.; Wang, Q.; Zhao, Y.; Wang, Z. Open pit limit optimization considering economic profit, ecological costs and social benefits. *Trans. Nonferrous Met. Soc. China* **2021**, *31*, 3847–3861. [CrossRef]
5. Wang, S.; Cao, B.; Bai, R.C.; Liu, G.W. Mid-long term boundary dynamic optimization of open-pit coal mine considering coal price fluctuation. *PLoS ONE* **2024**, *19*, e0296932. [CrossRef] [PubMed]
6. Zhang, C.; Zhao, G.B.; Zhang, J.P.; Tian, Y. Coordinated mining and pit boundary optimization for edge and stranded resources in Baorixile Open-pit Coal Mine. *Coal Eng.* **2025**, *57*, 23–30.
7. Lv, S.K.; Zhang, R.X.; Wang, Y.B.; Tao, Y.B.; Feng, J.C.; Meng, Z.J. Research on dynamic collaborative optimization and decision-making methods for composite coal seam open-pit mine bottom boundaries. *J. China Coal Soc.* **2025**, *50*, 9–19.
8. Li, J.W.; Xue, S.; Hou, Y.W.; Li, X.W.; Guo, J.L. A high-precision boundary identification method and its application to coal mine fire zone boundary interpretation. *J. China Coal Soc.* **2024**, *49*, 2757–2768.
9. Song, Z.L.; Wen, Y.; Jia, Z.Z. Analysis of the impact of rock joint cracks on blastability of burnt rock in Xinjiang open pit coal mines. *Sci. Rep.* **2025**, *15*, 16179. [CrossRef] [PubMed]
10. Cao, B.; Tao, Y.B.; Han, Y.; Zhang, Z.G.; Bai, W.Z.; Liu, Z.L. Division boundary optimization of inclined coal seam in open-pit mine under eroded burnt rock. *Coal Sci. Technol.* **2020**, *48*, 228–235.
11. Li, J.Y. Optimization Study of Coal Seam Blasting Scheme in Dananhu No. 2 Open Pit Mine. Master's Thesis, Liaoning Technical University, Fuxin, China, 2023.
12. Song, Z.L.; Jia, Z.Z.; Wen, Y. Blasting fragmentation mechanism and blasting parameter optimization of coal mine burned rock. *J. Liaoning Tech. Univ. (Nat. Sci. Ed.)* **2024**, *43*, 556–564.
13. Li, C.; Yan, J.; Zhao, J.S.; Li, W.; Guo, X.F. Study on seepage characteristics and mining stability of burnt rock slope. *China Coal* **2021**, *47*, 48–53.
14. Li, C.; Zhao, J.S.; Zhang, G.C. Influence and control of burnt rock groundwater on open-pit mining of Dannanhu No. 2 Mine. *Coal Eng.* **2017**, *49*, 46–49.
15. Wen, Y.; Song, Z.L.; Fan, J.F.; Zhao, X.L.; Zhang, Y.H.; Xia, S.Y.; Long, Y.F. Research on controlled mining of end slope fire-burned area in open-pit mine. *Sci. Rep.* **2024**, *14*, 21152. [CrossRef] [PubMed]
16. Liu, G.W.; Huang, Y.L.; Cao, B.; Yao, Y.; Wang, X.D.; Fu, E.S. Optimization of working slope configuration in seasonal operations of cold regions open-pit mine. *Alex. Eng. J.* **2024**, *87*, 533–542. [CrossRef]
17. Li, Q.S. Theoretical and Technical System of Ecological Open-Pit Coal Mining and Its Application. *J. China Coal Soc.* **2024**, *49*, 2426–2444.
18. Li, J.P.; Wang, W.C.; Wang, C.Y. Mechanism and control of slope instability slip induced by overburden migration in side coal mining. *Coal Sci. Technol.* **2025**, *53*, 127–143.

19. Ma, L.; Jin, X.Y.; Zhang, Q.F.; Jiang, K.S.; Li, M.B.; Hu, Y. Stability analysis of the inner dump with inclined base considering anti-slip pillar. *Coal Sci. Technol.* **2024**, *52*, 181–188.
20. Liu, G.W.; Huang, Y.L.; Cao, B.; Yao, Y. Dynamic control of working slope shape and optimization of advance speed in seasonally stripped open-pit coal mine. *Coal Sci. Technol.* **2023**, *51*, 45–54.
21. Wang, H.L.; Guo, X.; Zhang, Y.F.; Zhang, J.S. Research progress and application of online coal quality and coal quantity analyses. *Coal Sci. Technol.* **2024**, *52*, 219–237.
22. *GB/T 482-2008*; Sampling of Coal Seams. Standards Press of China: Beijing, China, 2008.
23. Wen, Y.; Song, Z.L.; Zhao, B.; Lv, M.J. Optimization of retaining ditch height for gentle slope turning in inclined coal seam open-pit mines. *Int. J. Energy Environ. Sci.* **2025**, *10*, 162–173. [CrossRef]
24. Wen, Y.; Song, Z.L.; Su, Q.; Liu, Z.W.; Wu, C.S.; Zhang, L. Optimization study on transverse mining zoning during the capacity expansion stage of nearly horizontal open-pit coal mines. *Sci. Rep.* **2026**, *16*, 3908. [CrossRef] [PubMed]
25. Xia, S.Y.; Song, Z.L.; Zhao, X.L.; Li, J.Y. Review of the recent advances in the prevention, treatment, and resource recovery of acid mine wastewater discharged in coal mines. *J. Water Process Eng.* **2023**, *52*, 103555. [CrossRef]
26. Jia, Z.Z.; Song, Z.L.; Fan, J.F.; Jiang, J.Y. Prediction of blasting fragmentation based on GWO-ELM. *Shock. Vib.* **2022**, *2022*, 7385456. [CrossRef]
27. Xia, S.Y.; Song, Z.L.; Zhao, X.L.; Ma, Z.M.; Li, J.Y. Study on preparation and properties of antifreeze compound road dust suppressant. *Sci. Rep.* **2024**, *14*, 16642. [CrossRef] [PubMed]
28. Jia, Z.Z.; Song, Z.L.; Fan, J.F.; Jiang, J.Y.; Guo, S.P. Numerical simulation study on dust suppression mechanism of burning rock blasting in open-pit mine. *Front. Earth Sci.* **2022**, *10*, 832650. [CrossRef]
29. Xia, S.Y.; Song, Z.L.; Zhao, X.L.; Gao, Z.; Wen, Y.; Li, Y.N. Preparation of a vegetable-oil film-type emulsion dust suppressant and adsorption performance study on road dust surface in open-pit coal mines. *Environ. Res.* **2025**, *278*, 121737. [CrossRef] [PubMed]
30. Jia, Z.Z.; Song, Z.L.; Zhao, X.L.; Fan, J.F.; Jiang, J.Y.; Wang, X.H. Dust transport law and dust suppression technology based on gas-solid two-phase flow. *Arab. J. Geosci.* **2021**, *14*, 1751. [CrossRef]
31. Mingliang, Z.; Rehman, A.U.; Asghar, Z.; Zeeshan, A.; Gorla, R.S.R. Predictive Modeling and Sensitivity Analysis of Thermodynamic Irreversibilities in Peristaltic Transport of Bingham Plastic Fluid in Porous Media Using Artificial Neural Networks and Response Surface Methodology. *Heat Transf.* **2025**, *55*, 1591–1607. [CrossRef]

Disclaimer/Publisher's Note: The statements, opinions and data contained in all publications are solely those of the individual author(s) and contributor(s) and not of MDPI and/or the editor(s). MDPI and/or the editor(s) disclaim responsibility for any injury to people or property resulting from any ideas, methods, instructions or products referred to in the content.